RESEARCH ARTICLE

Gene conversion facilitates the adaptive evolution of self-resistance in highly toxic newts

Kerry L Gendreau[1*], Angela D Hornsby[1,2], Michael TJ Hague[3], Joel W McGlothlin[1]

[1] Department of Biological Sciences, Virginia Tech, Blacksburg, United States; [2] Philip L. Wright Zoological Museum, Division of Biological Sciences, University of Montana, Missoula, United States; [3] Division of Biological Sciences, University of Montana, Missoula, MT, United States

[*] For correspondence: kerryg@vt.edu

Abstract *Taricha* newts contain high concentrations of the deadly toxin TTX as an antipredator defense, requiring them to be physiologically resistant to their own toxin. Here, we reconstruct the origins of TTX self-resistance by sequencing the voltage-gated sodium channel (*SCNA*) gene family, the target of TTX, in newts and related salamanders. We show that extreme resistance in newts consists of a mixture of ancient changes and lineage-specific substitutions and that the nonsynonymous substitution rate is elevated in newts, suggesting positive selection. We also identify a novel exon duplication within *SCN4A* encoding an expressed TTX-binding site. Two resistance-conferring changes within newts appear to have spread via nonallelic gene conversion: in one case, one codon was copied between paralogs, and in the second, multiple substitutions were homogenized between the duplicate exons of *SCN4A*. Our results demonstrate that gene conversion can accelerate the coordinated evolution of gene families in response to selection.

Introduction

Reconstructing the histories of complex adaptations and identifying their molecular underpinnings are two of the primary goals of evolutionary biology. Fitting evolutionary models to molecular sequences in a phylogenetic context can help piece together the key steps in adaptive evolution and uncover the relative contributions of selection and other evolutionary mechanisms to adaptive phenotypic evolution (Smith et al. 2020). Comparative studies of convergence, or the repeated evolution of characters within different lineages undergoing the same environmental challenges, provide powerful evidence of both adaptation and connections between genetic and phenotypic change (Losos 2011). Investigations into the molecular basis of convergence have revealed multiple occurrences of parallelism, where different lineages have evolved changes within the same proteins, and occasionally at the same amino acid sites, in response to shared selective pressures, such as insects that have evolved the ability to feed on toxic plants (Zhen et al. 2012) and populations of ducks and humans living at high elevations (Graham and McCracken 2019). Such patterns support important roles for both positive selection and constraint in the origin of complex adaptations (reviewed by Storz 2016).

Resistance to tetrodotoxin (TTX), a potent neurotoxin, has evolved convergently in several distantly related organisms, including pufferfish, snakes, and newts (reviewed by Soong and Venkatesh 2006; Toledo et al. 2016), and therefore offers an ideal system to investigate the molecular basis of adaptive evolution (Arbuckle et al. 2017). The genetic basis of TTX resistance, which is well established in tetrodotoxic puffer fish (Jost et al. 2008) and in snakes that consume TTX-bearing prey (Feldman et al. 2012; Geffeney et al. 2002; McGlothlin et al. 2014; McGlothlin et al. 2016), involves amino acid substitutions in the toxin's target, voltage-gated sodium channels (*SCNA* genes or Na_v proteins). Na_v channels are responsible for the initiation and propagation of action potentials in excitable cells and are composed of four homologous domains (DI–DIV), each comprising six transmembrane helices and an extracellular pore-loop region (the P-loop; Fux et al. 2018). The four homologous P-loops, one in each domain, form a pore within the membranes of excitable cells to selectively allow sodium ions to cross when the channel is open. TTX exerts its effects by binding to the P-loops of sensitive channels and preventing sodium entry into cells, thus blocking action potentials. Gene

Table 1. Nomenclature for voltage-gated sodium channel genes. Patterns of tissue expression are inferred from studies of gene orthologs in mammals (reviewed in Yu and Catterall 2003)

Gene name	Protein name	Tissue expression
SCN1A	$Na_V1.1$	Brain
SCN2A	$Na_V1.2$	Brain
SCN3A	$Na_V1.3$	Brain
SCN4A	$Na_V1.4$	Muscle
SCN5A	$Na_V1.5$	Heart
SCN8A	$Na_V1.6$	Brain / peripheral nervous system

duplication events have resulted in six *SCNA* paralogs, each with tissue-specific expression, that are shared across all tetrapods (Table 1), with additional lineage-specific duplications occurring in amniotes (Widmark et al. 2011; Zakon 2012). Because the structure of these paralogs is highly conserved, each has the potential to be blocked by TTX if it lacks resistance-conferring substitutions.

Species that possess or consume TTX must either have a full complement of resistant paralogs or otherwise shield sodium channels from contact with the toxin. Indeed, resistant substitutions are present in all eight of the *SCNA* genes within the genomes of multiple species of TTX-bearing pufferfish (from the family Tetraodontidae; Jost et al. 2008) and in six of the nine *SCNA* genes in *Thamnophis sirtalis* snakes that consume TTX-bearing *Taricha* newts (McGlothlin et al. 2014; Perry et al. 2018). The three brain channels *SCN1A, SCN2A,* and *SCN3A* of snakes remain TTX sensitive, but presumably are protected from TTX by the blood-brain barrier (McGlothlin et al. 2014). In snakes, the evolution of extreme TTX resistance appears to follow a predictable, stepwise substitution pattern across TTX-exposed members of the *SCNA* gene family, with substitutions in heart and peripheral nerve channels preceding those in the muscle channel gene, *SCN4A*, which evolves resistance only in snakes locked in coevolutionary arms races with highly tetrodotoxic amphibian prey (Feldman et al. 2012; McGlothlin et al. 2016; Perry et al. 2018).

Less is known about the evolutionary history of TTX resistance in *Taricha* newts, the highly toxic coevolutionary partner of *Thamnophis* (Brodie and Brodie 1990; Brodie et al. 2002; Hague et al. 2020; Williams et al. 2010). The extreme toxicity of *Taricha*, which has been

77 elaborated by the ongoing coevolutionary arms race with garter snakes, builds upon lower levels
78 of toxicity that evolved ~40 million years ago (mya) within "modern" newts (tribe Molgini;
79 Hanifin and Gilly 2015; divergence date estimated by Hime et al. 2021). The evolution of
80 toxicity necessitates the evolution of toxin autoresistance so that a prey species is not
81 incapacitated by its own antipredator defense (Jost et al. 2008; Márquez et al. 2019; Tarvin et al.
82 2017; Toledo et al. 2016). Understanding the timing and details of this autoresistance can shed
83 light on the genetic processes underlying the predator-prey arms race. Hanifin and Gilly (2015)
84 compared the sequences of one sodium channel gene, the muscle paralog *SCN4A*, across several
85 salamander species and identified substitutions in the P-loops of DIII and DIV that provide
86 extreme TTX resistance to the muscles of TTX-bearing newts. Importantly, the sister group of
87 toxic newts had substitutions in the same gene providing more moderate resistance, indicating
88 that the evolution of autoresistance in a common ancestor paved the way for the evolution of
89 extreme toxicity. More recently, Vaelli et al. (2020) used transcriptome sequencing to
90 characterize the genetic basis of physiological resistance to TTX in *Taricha granulosa* and
91 identified substitutions within TTX-binding regions in the other five *SCNA* paralogs, many of
92 which occur in within the P-loop of DI. However, because it is unknown whether other
93 salamander species possess TTX resistance in these paralogs, the order and timing of the
94 evolutionary events leading to autoresistance in toxic newts is still unknown. Furthermore, no
95 studies to date have applied evolutionary models to test for the relative importance of
96 mechanisms such as positive selection, relaxed constraint, and interlocus gene conversion in the
97 evolution of newt TTX resistance.

98 Here, we trace the evolutionary history of the entire *SCNA* gene family across the
99 salamander phylogeny to show the order in which resistant substitutions appeared. Using
100 published genome sequences and newly generated sequence data, we characterize the genomic
101 structure of *SCNA* genes in newts and their relatives, inferring the timing of resistant
102 substitutions leading to the extreme TTX resistance observed across all *SCNA* paralogs in
103 *Taricha* newts (Vaelli et al. 2020). We estimate rates of synonymous and nonsynonymous
104 substitution to identify positive selection. In addition, we assess the potential of nonallelic gene
105 conversion, a process by which sequence is copied from one paralog to another (Chen et al.
106 2007), to act as a source of adaptive variation. Combining these data provides insight into the
107 evolutionary mechanisms underlying the origin of a uniquely potent chemical defense.

Results

Genomic structure and phylogenetics of voltage-gated sodium channels

We used targeted sequence capture to characterize *SCNA* sequences from the genomes of five salamander species (order Urodela), including three TTX-bearing newts (family Salamandridae, subfamily Pleurodelinae, tribe Molgini), *Notophthalmus viridescens*, *Taricha torosa*, and *Taricha granulosa* (n = 3 diploid individuals of each species), and two less toxic salamanders, *Cryptobranchus alleganiensis* (Crypotobranchidae) and *Plethodon cinereus* (Plethodontidae, n = 2 each). We also identified *SCNA* sequences within two publicly available salamander genome sequences: *Ambystoma mexicanum* (Ambystomatidae; Smith et al. 2019; AmexG.v6 assembly) and *Pleurodeles waltl* (Salamandridae; Elewa et al. 2017) and a full-body transcriptome from the fire salamander *Salamandra salamandra* (Salamandridae; Goedbloed et al. 2017; BioProject accession PRJNA607429). The split between *Cryptobranchus* (suborder Cryptobranchoidea) and all the other salamanders in our study (members of suborder Salamandroidea) represents the most ancient division in the phylogeny of extant salamanders (~160 mya; Hime et al. 2021).

We identified six *SCNA* genes in the genomes of all salamander species, which is consistent with observations in other amphibians (Zakon et al. 2011). We obtained near full-length assemblies for all paralogs (Table S1); however, a few exons containing TTX-binding sites, including exon 15 (encoding the DII P-loop) of *SCN2A* from *N. viridescens* and exon 22 (encoding part of the DIII P-loop) of *SCN2A* for several newt species, were missing from our assemblies. Polymorphism was rare in our assemblies and we observed few nonsynonymous mutations within the newt genomes, but we found slightly elevated polymorphism in *N. viridescens* relative to other species (Table S2). No nonsynonymous polymorphisms were observed within any of the known TTX-binding P-loop regions within any of the species sequenced for this study.

Synteny of *SCNA* genes in *A. mexicanum* is conserved relative to other tetrapods (Fig. S1), which allowed us to use the *A. mexicanum* sequences as a baseline to confidently identify *SCNA* paralogs in all species. Three of the paralogs, *SCN1A*, *SCN2A*, and *SCN3A* are arrayed in tandem on *A. mexicanum* chromosome 9, with *SCN2A* inverted relative to its neighboring paralogs (Table 2, Fig. S1). The additional three paralogs, *SCN4A*, *SCN5A*, and *SCN8A*, are each located on separate chromosomes (Table 2). In the gene family tree built from amino acid sequences, all salamander Na_v1 proteins formed a monophyletic clade with the corresponding

orthologs from the genomes of the frogs *Xenopus tropicalis* and *Nanorana parkeri*, which we included as outgroups (Fig. 1). The gene family tree constructed from the nucleotide coding sequences of these genes yielded a similar topology, with each salamander *SCNA* ortholog forming a monophyletic clade. However, in the nucleotide gene family tree, the three *X. tropicalis* nerve channels $Na_v1.1$, $Na_v1.2$, and $Na_v1.3$ formed a monophyletic clade that is distinct from the salamander sequences (Fig. S2).

Table 2. Locations of voltage-gated sodium channel genes in the *Ambystoma mexicanum* AmexG.v6 genome assembly

Gene	Chromosome	Start	End	Strand	Length (bp)
SCN1A	9q	503,107,904	503,797,933	+	690,029
SCN2A	9q	507,685,503	508,688,108	-	1,002,605
SCN3A	9q	509,830,827	510,576,927	+	746,100
SCN4A	13q	113,343,821	115,707,581	+	2,363,760
SCN4A exon 26b	13q	115,891,071	115,892,251	+	1,180
SCN5A	2p	562,159,042	563,030,267	-	871,225
SCN8A	3q	465,212,114	466,692,047	-	1,479,933

Partial duplication of *SCN4A* and evolution of TTX resistance in duplicated domains

Our search of the *A. mexicanum* genome revealed a partial tandem duplication of the 3' end of the *SCN4A* gene, including the full coding region of exon 26, located ~180,000 base pairs downstream of the full-length *SCN4A* gene on the same DNA strand (Table 2). Both exon 26 copies are similar in length to each other and to exon 26 of other paralogs, encoding open reading frames of approximately 390 base pairs without introduced stop codons. Exon 26 is the 3'-terminal exon of the *SCN4A* gene and encodes the TTX-binding P-loop region of DIV. Hereafter, we refer to the duplicate exons as 26a (more proximal to exon 25) and 26b (more distal to exon 25) and duplicate P-loop regions as DIVa (more proximal to exon 25) and DIVb (more distal to exon 25). We also found this duplicated exon in *SCN4A* orthologs within the genomes of salamanders *P. cinereus*, *P. waltl*, *N. viridescens*, *T. torosa*, and *T. granulosa* and in published transcriptomes of *Tylototriton wenxianensis* and *Bolitoglossa vallecula*, but not in the transcriptome of *Hynobius retardatus* or in the genomes of *C. alleganiensis* or the frogs *X. tropicalis* or *N. parkeri*. This pattern suggests that the duplication event likely took place after

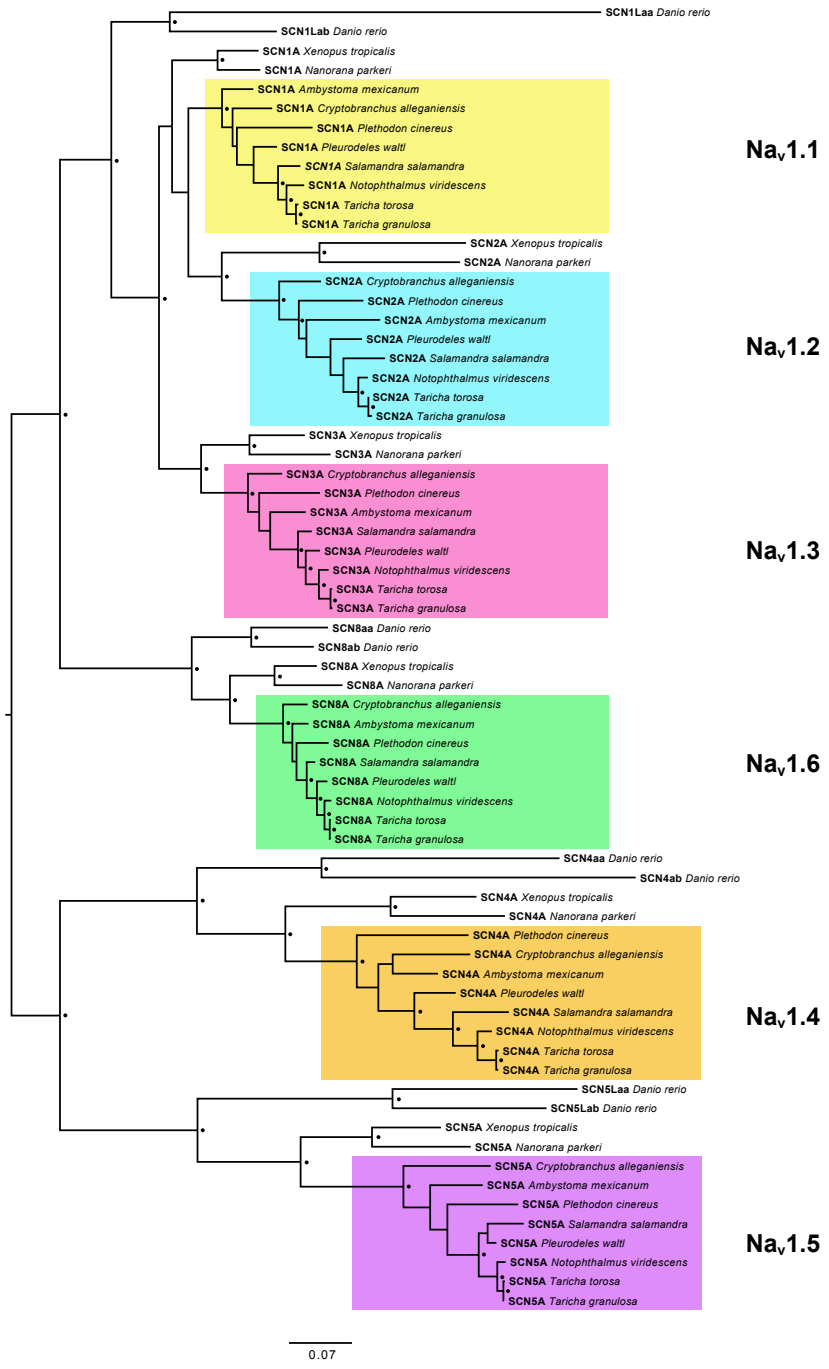

Figure 1. Evolutionary relationships among salamander voltage-gated sodium channels. Midpoint rooted maximum likelihood tree constructed from alignment of 2188 amino acids from full coding sequence translations of salamander sodium channel genes, including sequences from two frogs (*Nanorana parkeri* and *Xenopus tropicalis*) and one fish (*Danio rerio*) as outgroups. Black circles indicate nodes with >90% bootstrap support.

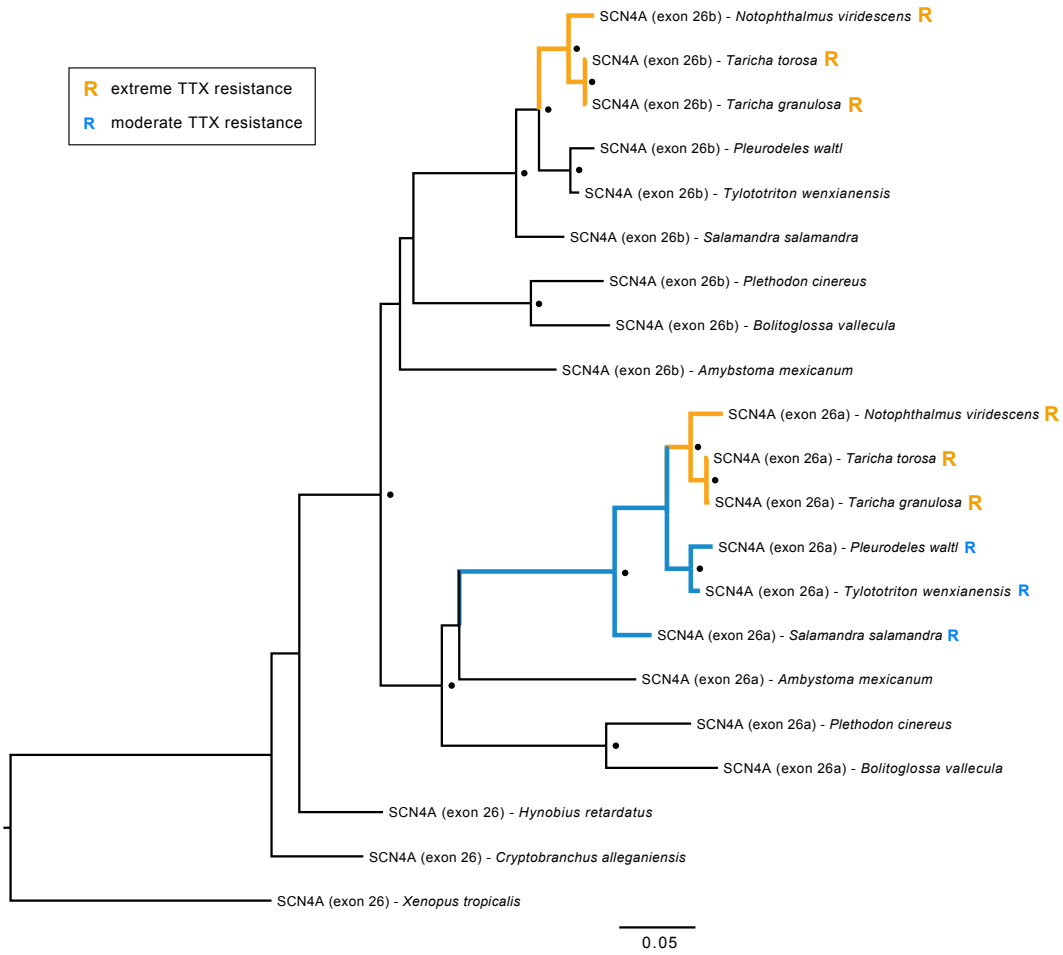

Figure 2. Ancestral duplication and convergent evolution of TTX resistance in *SCN4A* terminal exon 26. Maximum likelihood tree constructed from 1050 bp nucleotide alignment of *SCN4A* exon 26 identified in salamander genomes and transcriptomes. “Exon 26a” and “exon 26b” in tip labels refer to the exon copy more proximal and more distal to exon 25, respectively. Black circles indicate node bootstrap support >95%. “R” at tips indicates the presence of substitutions conferring extreme (orange) and moderate (blue) TTX resistance.

the split of Cryptobranchoidea and Salamandroidea (Fig. 2). Within the *S. salamandra* transcriptome, we found four unique RNA sequences transcribed from the *SCN4A* locus, with alternative splicing of exon 17 and alternative encoding of either exon 26a or 26b. Genome-mapped reads of multi-tissue transcriptomes of *A. mexicanum* (Bryant et al. 2017; Caballero-Pérez et al. 2018; Nowoshilow et al. 2018) indicate that these alternative transcripts have similar expression profiles across various tissues. Taken together, these observations provide evidence that the duplication of exon 26 led to the creation of functional splice variants in these salamanders.

While numerous nonsynonymous substitutions differentiated the duplicated *SCN4A* exon 26 sequences relative to the original sequences within each genome, we found that identical substitutions conferring extreme TTX-resistance to toxic newts (Hanifin and Gilly 2015) were present in both exons from the genomes of all three TTX-bearing newts but not in other, less toxic salamander species (Fig. 2). Also consistent with the results of Hanifin and Gilly (2015), we found resistant substitutions conferring moderate TTX resistance in exon 26a of *P. waltl*, *T. wenxianensis*, and *S. salamandra*; however, we observed no resistant substitutions in exon 26b outside of the toxic newt clade.

Evolution of TTX resistance in salamanders

We characterized levels of TTX resistance in each Na_v paralog as extreme, moderate, and TTX-sensitive based on previous site-directed mutagenesis experiments in which substitutions were introduced to TTX-sensitive Na_v channels and cross-membrane Na^+ current was measured *in vitro* in the presence and absence of TTX (Table 3). Our results confirm that *T. granulosa* has six paralogs with extreme TTX resistance (Table 3, Fig. 3). Our findings are consistent with those reported by Vaelli et al. (2020) with one exception: we associate DIV (encoded by exon 26) substitutions A1529G and G1533V with $Na_v1.1$ and Q1524E and G1533R with $Na_v1.2$ based on synteny mapping (Fig. S1), gene trees (Figs. 1, S2), and alignments of exon 26 (Fig. S3), whereas the previous study reversed these assignments. We also show that substitutions with extreme TTX resistance are present in all six Na_v paralogs in two other species of highly toxic newt, *T. torosa* and *N. viridescens*, indicating that the common ancestor of these three species possessed extreme TTX resistance. Many of the substitutions in toxic newts parallel those found in TTX-bearing fish and in snakes that consume tetrodotoxic amphibians (Table 3).

Table 3. List of TTX resistance-conferring substitutions observed in salamanders. Listed are all substitutions observed in salamander Na_v channels that are known to confer TTX resistance. Parallel substitutions in observed in Na_v channels of TTX-bearing pufferfish and in snakes that consume TTX-bearing prey are also shown. Resistance categories for all substitutions except those in muscle channel $Na_v1.4$ (marked with asterisks) are based on fold-change in TTX sensitivity, which was determined by calculating the ratio of IC_{50} values (the TTX concentration at which 50% of Na_v channels are blocked by TTX i*n vitro*) of the mutated and wild-type channels. Resistance categorization for $Na_v1.4$ substitutions was inferred from Hanifin and Gilly (2015), who measured the direct impact of TTX exposure on the action potentials of salamander muscle fibers. Amino acid sites are in reference to rat $Na_v1.4$ (accession number AAA41682).

Substitution	Tetrodotoxic newts	Non-tetrodotoxic salamanders	Pufferfish and snakes	Fold-change in TTX sensitivity	Resistance category	Citation
Y401C (DI)	$Na_v1.1$ $Na_v1.2$	$Na_v1.5$	Pufferfish: $Na_v1.4a$ $Na_v1.5La$ $Na_v1.5Lb$	~2500×	Extreme	Jost et al. (2008); Venkatesh et al. (2005)
Y401A (DI)	$Na_v1.1$ $Na_v1.3$ $Na_v1.6$	$Na_v1.1$	Pufferfish: $Na_v1.1La$ $Na_v1.6b$	>600×	Extreme	Jost et al. (2008); Vaelli et al. (2020)
Y401S (DI)	$Na_v1.5$	$Na_v1.5$	-	~7000×	Extreme	Leffler et al. (2005)
D1532S (DIV) G1533D (DIV)	$Na_v1.4$		Snake: $Na_v1.4$	-	Extreme*	Feldman et al. (2012); Hanifin and Gilly (2015)
E758D (DII)	-	$Na_v1.5$	Pufferfish: $Na_v1.4b$	~3000×	Extreme	Bricelj et al. (2005)
M1240T (DIII)	$Na_v1.1$ $Na_v1.4$	$Na_v1.1$ $Na_v1.5$	Pufferfish: $Na_v1.1La$ $Na_v1.1Lb$ $Na_v1.4a$ $Na_v1.4b$	~15×	Moderate	Jost et al. (2008)
V1233I (DIII)	$Na_v1.6$	$Na_v1.6$	Snake: $Na_v1.6$	~2×	Moderate	McGlothlin et al. (2014); Vaelli et al. (2020)
I1525V (DIV)	$Na_v1.6$	$Na_v1.5$ $Na_v1.6$	Snake: $Na_v1.6$	~2×	Moderate	Geffeney et al. (2005); McGlothlin et al. (2014); Vaelli et al. (2020)
I1525S (DIV)	$Na_v1.4$	$Na_v1.4$		-	Moderate*	Hanifin and Gilly (2015)
I1525T (DIV)	-	$Na_v1.4$ $Na_v1.5$		~7.7×	Moderate	Du et al. (2009)

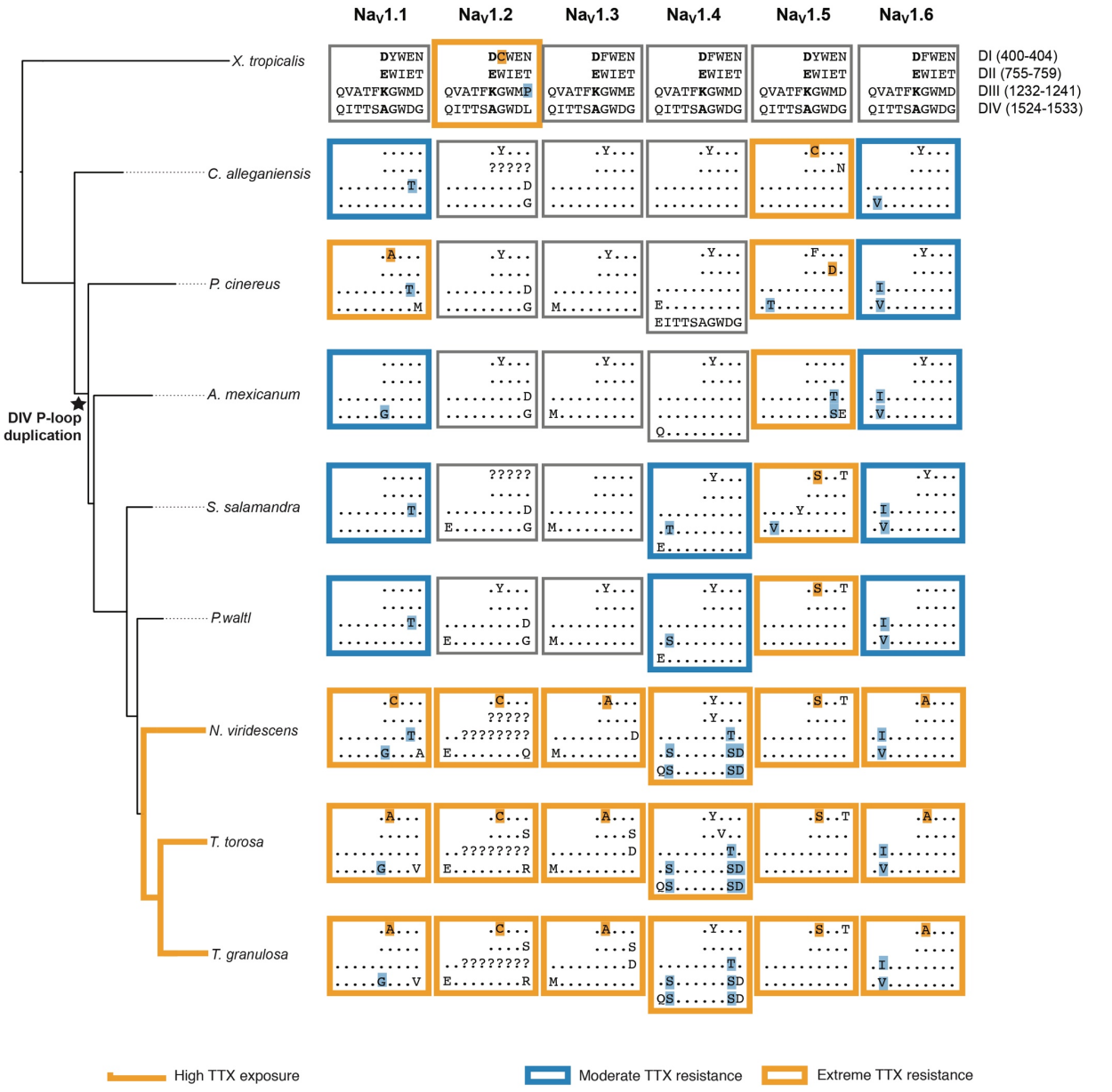

Figure 3. Distribution of TTX-resistance conferring substitutions in salamander voltage-gated sodium channels. Toxic newt species are indicated with orange branches ("High TTX exposure"). Amino acids associated with Na+ selectivity (400D, 755E, 1237K, 1529A) are shown in bold. Dots indicate identity with consensus sequences. Blue boxes indicate paralogs inferred to have moderate (~2-15-fold) resistance, orange boxes indicate paralogs with extreme (>300-fold) resistance, and grey boxes indicate paralogs without resistance or with insufficient sequence data. Substitutions known to confer TTX resistance are highlighted with respective colors. Extreme resistance in a paralog can result from the presence of one highly resistant substitution or the combination of multiple moderately resistant substitutions. Exon duplication has led to an additional TTX-binding domain (DIVb) in Na$_v$1.4 of all salamanders except *C. alleganiensis*. We did not identify the sequence encoding DIII of *SCN2A* for any of the newts, however Vaelli et al. (2020) report that, in *T. granulosa*, this domain is identical in amino acid sequence to other salamanders. Amino acid sites are in reference to rat Na$_v$1.4 (accession number AAA41682).

No salamander species outside the clade of highly toxic newts possessed a full complement of TTX-resistant Na_v paralogs, indicating the evolution of full physiological resistance coincided with the origin of extreme toxicity. However, we found at least three paralogs with moderate or extreme TTX resistance in all salamander species we examined, indicating that the evolution of TTX resistance in newts built upon more ancient changes that first appeared in their non-newt relatives. Substitutions conferring moderate or extreme resistance were observed within the heart channel $Na_v1.5$ and brain/nerve channels $Na_v1.1$ and $Na_v1.6$ of all salamander species, with additional resistance-conferring substitutions evolving within TTX-bearing newts. As first shown by Hanifin and Gilly (2015), moderate resistance was present in the skeletal muscle channel $Na_v1.4$ of *S. salamandra* and *P. waltl*, but not in the three other salamander species we examined. Although our outgroup, the frog *X. tropicalis*, also contained a highly resistant substitution in $Na_v1.2$, we found no evidence for resistance in this paralog in any salamanders outside of tetrodotoxic newts.

Based on our ancestral sequence reconstructions, the most recent common ancestor of all salamanders had three TTX resistant sodium channels: $Na_v1.1$ (brain, moderately resistant), $Na_v1.5$ (heart, highly resistant), and $Na_v1.6$ (brain/peripheral nerves, moderately resistant; Fig. 3). Moderate resistance in the muscle channel $Na_v1.4$ appeared between 75–130 mya, after the divergence of Ambystomatidae and Salamandridae (the family consisting of true salamanders and newts; Hanifin and Gilly 2015). This gain in muscle resistance coincided with the appearance of two highly resistant substitutions in DI of $Na_v1.5$, which are present in all Salamandridae. Extreme TTX resistance across all *SCNA* paralogs evolved more recently, occurring approximately 37–50 mya, after the split between primitive newts – which include *Pleurodeles* – and modern newts, which include all TTX-bearing species. Over this time period, TTX resistance evolved in $Na_v1.2$ and $Na_v1.3$, and multiple additional resistant mutations appeared and became fixed in $Na_v1.1$, $Na_v1.4$, and $Na_v1.6$.

Selective regimes and evolutionary rates

In order to characterize the selective regimes acting on *SCNA* genes, we used the codeml program in PAML (Yang 2007) to fit models of selection to *SCNA* codon alignments and compared nested models using likelihood ratio tests (LRTs). We tested for site-specific positive selection within all amphibians by comparing two sets of nested models: one set using a discrete

distribution of ω values either with or without positive selection (M1a vs. M2a; Yang et al. 2005); and another set fitting a continuous distribution of ω values under purifying selection only, or adding categories of unconstrained evolution and positive selection (M7 vs. M8 and M8a vs. M8; Yang et al. 2000). Parameter estimates and LRT results for site models are summarized in Table S3. To test for selection within toxic newts, we fit branch (Yang 1998) and branch-site models (Zhang et al. 2005) to our datasets, which allowed ω to vary both among codon sites and between toxic newts and other amphibians (summarized in Table S4).

All models estimated relatively low ratios of nonsynonymous to synonymous substitution (d_N/d_S, or ω ratios) for all Na_v paralogs (average ω ratios from branch models ranged from 0.05 to 0.25), indicating pervasive purifying selection. Based on LRTs comparing one ω-value models (which allow only for one ω value across the entire phylogeny) to branch models (allowing for a different ω ratio in the toxic newt clade relative to other amphibians), we found that ω ratios were significantly higher in toxic newts for $Na_v1.1$, $Na_v1.3$, and $Na_v1.4$, borderline significant for $Na_v1.6$, and non-significant for $Na_v1.2$ and $Na_v1.5$ (Fig. 4A; Table S4). The largest difference in ω ratios in the branch test was observed for the muscle channel $Na_v1.4$ (newt ω = 0.25; all salamanders ω = 0.10), which appears to be due to both an increase in the proportion of unconstrained sites as well as a larger number of estimated sites undergoing positive selection (Fig. 4B). However, the posterior probability support for positive selection at many of these sites was low, and LRTs from branch-site models indicated significant evidence for a shift in positive selection only in paralog $Na_v1.3$ (Tables S3, S4).

Our site and branch-site models identified a number of TTX-binding sites with elevated ω ratios (Table 4; Tables S5, S6). Because of the small number of species in our study, we had low power to detect statistically significant positive selection (Anisimova et al. 2001; Kosakovsky Pond and Frost 2005; Yang et al. 2000), and the posterior probabilities provided low-to-moderate support for positive selection at most sites. We also note that the false positive rates of site selection models can be inflated due to gene conversion events (Casola and Hahn 2009), among-site variation in d_S (Kosakovsky Pond and Frost 2005), and multinucleotide mutations (Venkat et al. 2018). However, results were consistent between the M2a and M8 models, and the codons that were identified suggest that positive selection may have been important for observed substitutions in TTX-binding regions.

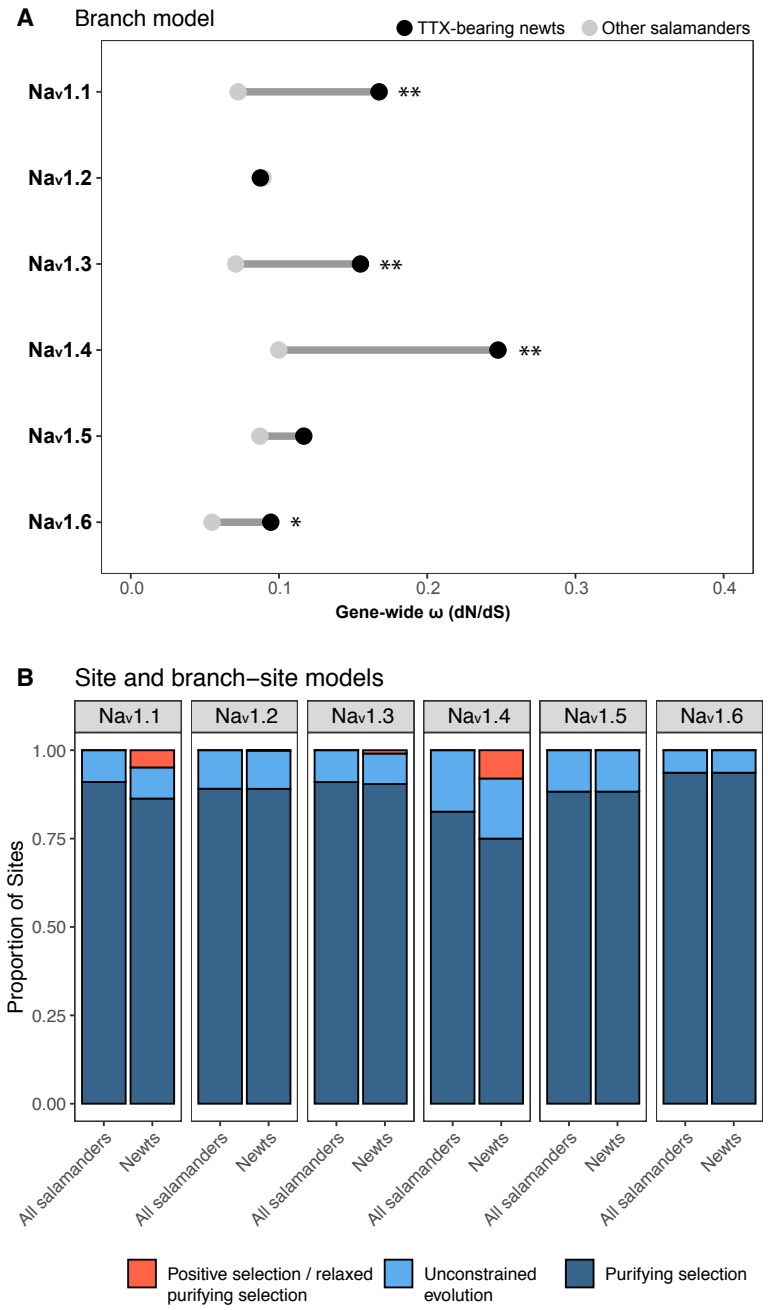

Figure 4. Tests for shifts in selective pressure on salamander voltage-gated sodium channels. (A) PAML branch models comparing estimates of gene-wide ω (d_N/d_S) within TTX-bearing newts (black circles) and other salamanders (grey circles). Significant differences based on likelihood ratio tests are indicated with * ($p < 0.05$) and ** ($p < 0.01$). (B) PAML site and branch-site model estimates of proportions of sites under purifying selection ($0 < \omega < 0.05$ in both lineages), unconstrained evolution ($\omega = 1$ in both lineages), and positive selection or relaxed purifying selection ($0 < \omega < 0.05$ in salamanders and $\omega \geq 1$ in TTX-bearing newts). Although likelihood-ratio tests were non-significant for Na$_V$1.1 and Na$_V$1.4 (Tables S3, S4), PAML identified a large proportion of amino acid coding sites within these paralogs with elevated d_N/d_S ratios in toxic newts.

Table 4. P-loop sites with elevated ω values in all salamanders and in toxic newts. Sites were detected as putatively affected by positively selection within salamanders and within toxic newts using the empirical Bayes method based on site models and branch-site models respectively. Because we had low power to detect positive selection at specific sites due to the small number of species in our study, these results should be interpreted with caution. Included are all P-loop sites identified as putatively positively selected with posterior probability > 0.50. Sites with posterior probability > 0.95 are indicated with asterisks, but we note that the likelihood ration test for the $Na_v1.4$ branch-site model was non-significant. Bolded sites have non-conservative amino acid substitutions associated with TTX resistance in toxic newts.

	$Na_v1.1$	**$Na_v1.2$**	**$Na_v1.3$**	**$Na_v1.4$**	**$Na_v1.5$**	**$Na_v1.6$**
Tissue expression	Brain	Brain	Brain	Muscle	Heart	Brain / PNS
P-loop sites under positive selection in all salamanders	**Y401A/C (DI)** **G1533V (DIV)**	**G1533R (DIV)**	**Y401A (DI)**	-	739 (DII)	**Y401A (DI)**
P-loop sites under positive selection in toxic newts	1224 (DIII) **A1529G (DIV)**	-	T759S (DII)	W756Y (DII)* **M1240T (DIII)** 1517 (DIV) 1519 (DIV) **D1532S (DIV)***	-	-

Within the brain channels $Na_v1.1$, $Na_v1.3$, and $Na_v1.6$, putative positive selection was detected by site models at site 401 within the DI P-loop, indicating selection acting across all salamanders rather than specifically within toxic newts (Table 4). Replacement of the aromatic amino acid at site 401 with a non-aromatic amino acid can substantially impact TTX binding capacity (Leffler et al. 2005; Vaelli et al. 2020; Venkatesh et al. 2005), and we observed non-aromatic substitutions at this site within all brain channels of highly toxic newts (Fig. 3, Table 3). The codon sequence for site 401 was variable across many salamanders lacking TTX; however, almost all of the nonsynonymous changes observed outside of TTX-bearing newts were biochemically conservative (both phenylalanine and tyrosine are aromatic and do not affect TTX binding; Sunami et al. 2000), with the exception of the 401A observed in *P. cinereus* $Na_v1.1$. This conservative variation likely contributes to the signal of diversifying selection acting on this codon in less toxic salamander lineages. Site models also suggested positive selection acting on site 1533 in DIV of $Na_v1.1$ and $Na_v1.2$ (Table 4). Although the substitutions present at site 1533 in these newt paralogs have not been tested experimentally for their effects on TTX binding,

Maruta et al. (2008) showed that a G1533T substitution at this site led to a moderate (~2-3-fold) decrease in TTX binding affinity, and substitutions at this site are common in TTX-resistant channels (Feldman et al. 2012; Geffeney et al. 2005; Jost et al. 2008; McGlothlin et al. 2016), suggesting that these non-synonymous changes likely also reduce TTX binding affinity in newts.

Within the toxic newt lineage, we identified putative positive selection acting on three known TTX-binding sites: 1240 and 1532 in DIII and DIV of muscle channel $Na_v1.4$ and 1529 in DIV of brain channel $Na_v1.1$ (Table 4). In $Na_v1.4$, sites 1240 and 1532 contain resistance-conferring substitutions exclusively within toxic newts and these substitutions have been associated with extreme TTX resistance in *Taricha* muscle fibers (Hanifin and Gilly 2015). In $Na_v1.1$, site 1529 encodes part of the Na^+ selectivity filter (comprised of interacting amino acids DEKA – sites 400, 755, 1237, and 1529), which is highly conserved across Na_v paralogs. An A1529G substitution (resulting in a DEKG filter) is present in $Na_v1.1$ of *A. mexicanum* and all members of the toxic newt clade. While this substitution does not appear to affect Na+ selectivity or to be sufficient in preventing TTX from binding (Jost et al. 2008), it can alter channel firing properties, producing substantially higher Na^+ currents in comparison to the DEKA filter (Jost et al. 2008). The same alanine to glycine substitution has been observed in Na_v channels of TTX-bearing flatworms (Jeziorski et al. 1997) and pufferfish (Jost et al. 2008), which suggests that it may play a role in TTX resistance in these organisms.

Outside of TTX-binding regions, we found evidence for putative positive selection in similar regions across multiple *SCNA* paralogs (Tables S5, S6). For $Na_v1.4$, the majority of sites under positive selection reside in terminal exon 26a that encodes the DIVa P-loop (exon 26b was excluded from this analysis due to its absence in some species). For most other paralogs, the largest clusters of sites with elevated d_N/d_S ratios occurred within the DI L5 turret (the extracellular loop upstream of the DI P-loop, encoded by exons 6 and 7) and/or within the DIII L5 turret upstream of the DIII P-loop encoded by exon 21. These sites may facilitate interaction with other proteins, or alternatively, some of these sites identified by the branch-site model may be selected to compensate for biochemical changes produced by TTX-resistant mutations.

Gene conversion events

We also tested for evidence of nonallelic gene conversion as a mechanism of sequence evolution contributing to adaptive evolution in *SCNA*s using the program GENECONV. Nonallelic or

297 ectopic gene conversion results from an interlocus exchange of DNA that can occur between
298 closely related sequences during double-stranded break repair (Hansen et al. 2000).
299 GENECONV uses the information in a multiple sequence alignment to identify regions of
300 similarity shared between two sequences that is higher than expected by chance based on
301 comparisons to permuted alignments (Sawyer 1999). We selected this program to detect gene
302 conversion because of its low false positive rates and robustness to shifts in selective pressure
303 (Bay and Bielawski 2011; Posada and Crandall 2001). Because nonallelic gene conversion is
304 more likely to occur between paralogs residing on the same chromosome (Benovoy and Drouin
305 2009; Drouin 2002; Semple and Wolfe 1999), we limited our search to events between the
306 tandem duplicates *SCN1A*, *SCN2A*, and *SCN3A* and between exons 26a and 26b of *SCN4A*
307 within each salamander genome. While few gene conversion events were detected within each
308 species by GENECONV, all of the regions that were detected within *Taricha* newts contain
309 TTX-binding sites with substitutions associated with TTX resistance, including the DIVa and
310 DIVb P-loops of *SCN4A* (Fig. 5; Table 5). We observed three TTX resistant amino acids
311 (I1525S, D1532S, G1533D) within the DIVa and DIVb P-loops of *SCN4A* in toxic newt
312 genomes. In contrast, *P. waltl*, a closely related but non-tetrodotoxic newt, contains one
313 moderately TTX-resistant amino acid (I1525S) in the DIVa P-loop and no resistant amino acids
314 in the DIVb P-loop (Fig. 5A). These differences involve four identical nucleotide changes at
315 homologous sites in both exon duplicates. Our short reads from the genomes of *N. viridescens*
316 and *Taricha* newts mapped onto each of these exon assemblies across putative recombination
317 break points with high (> 50-fold) coverage, lending support for sequence convergence rather
318 than an assembly error. We did not detect gene conversion between these exons within the
319 genomes of *T. granulosa* or *N. viridescens*; however, this may be due to the low power of
320 GENECONV to detect conversion (Bay and Bielawski 2011), particularly in the presence of low
321 sequence diversity and when the conversion tract is shorter than ~100 bp (McGrath et al. 2009;
322 Posada and Crandall 2001). Together, these results suggest that the three resistant amino acids
323 accumulated together in one exon copy followed by conversion of the other exon ~40 mya in a
324 toxic newt ancestor.

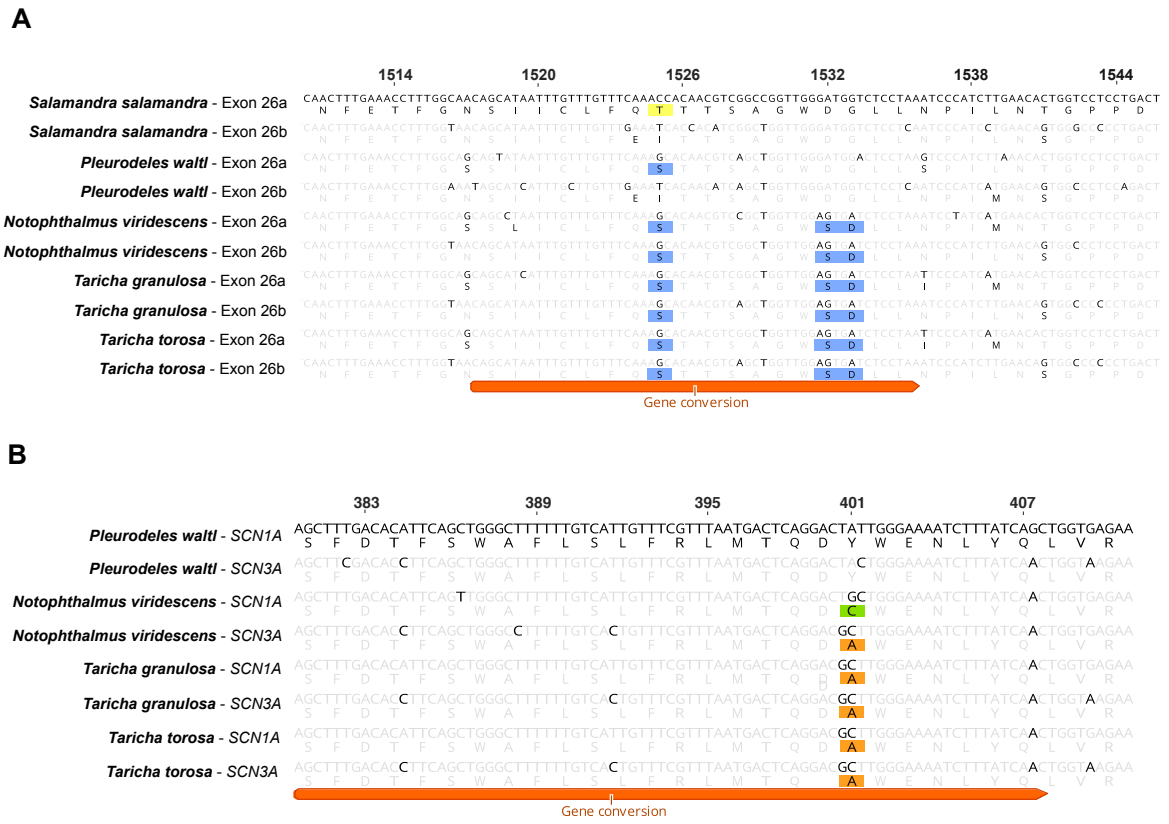

Figure 5. Gene conversion within TTX binding regions. (A) Gene conversion was detected between DIVa and DIVb P-loops within duplicate exons 26a and 26b of *SCN4A* in *T. torosa*. Substitutions conferring TTX resistance are highlighted in yellow and blue. While one moderately resistant substitution is present in DIVa of less toxic salamanders (1525T/S), three identical substitutions are present in both DIVa and DIVb of highly toxic newts. (B) Gene conversion was also detected between the DI P-loops of paralogs *SCN1A* and *SCN3A* in both *T. torosa* and *T. granulosa*. In *Notophthalmus*, both paralogs have different resistant substitutions (401C in *SCN1A* – highlighted in green; 401A in *SCN3A* – highlighted in orange). This putative gene conversion may have homogenized TTX-resistant substitutions among these paralogs within *Taricha* newts. Site numbers are in reference to amino acids of rat $Na_v1.4$ (accession number AAA41682).

We also detected gene conversion between the DI P-loops of paralogs *SCN1A* and *SCN3A* within the genomes of both *Taricha* species (Fig. 5B, Table 5). TTX-resistant substitutions are identical in the DI P-loops of *SCN1A* and *SCN3A* in both *Taricha* species (401A, encoded by a GCT codon), while *SCN1A* of *N. viridescens* contains a different codon at this position (TGC, encoding 401C), consistent with gene conversion occurring at this locus in *Taricha.* Both *SCN1A* and *SCN3A* of non-tetrodotoxic *P. waltl* newts encode a TTX-sensitive tyrosine at this locus. It is unclear whether putative gene conversion event(s) occurred before or after resistance evolved in both paralogs. Gene conversion may have converted a non-resistant channel to a resistant channel in an ancestral *Taricha*, while *N. viridescens* independently acquired a Y401A substitution, or it may have homogenized substitutions within two channels that had previously evolved resistance in an ancestor of all toxic newts. In *Taricha* newts, the transition from either tyrosine or cysteine to alanine required multiple nucleotide substitutions in both paralogs, making gene conversion a likely explanation for the observed substitution patterns.

We detected additional gene conversion events that may have involved a non-resistant paralog acting as a donor to a resistant paralog, leading to the loss of TTX resistance in *A. mexicanum* and *C. alleganiensis* paralogs. A resistant substitution is present in the DIII P-loop of *SCN1A* in most salamanders but is absent in *SCN1A* of *A. mexicanum* (Fig. 3), and we detected gene conversion in an adjacent region between *SCN1A* and the non-resistant *SCN2A* paralog within the *A. mexicanum* genome (Table 5). Similarly, *C. alleganiensis SCN2A* contains a non-resistant 1533G within DIV of all six paralogs, while *SCN2A* of *X. tropicalis* frogs encodes a putatively TTX-resistant 1533L, and gene conversion between paralogs *SCN2A* and *SCN3A* may have facilitated the loss of this substitution in salamanders

.

Table 5. Gene conversion events between adjacent salamander voltage-gated sodium channel paralogs detected with GENECONV. Bolded rows indicate putative gene conversion events associated with the gain (*) or loss (†) of TTX resistance substitutions within a lineage. Global Bonferroni-corrected (BC) p-values from 10,000 simulations are reported. Protein begin and end sites reference the rat $Na_v1.4$ channel (accession number AAA41682). Total poly – polymorphism within the converted region across all species; num diffs – pairwise differences between the two paralogs within the converted region; total diffs – total pairwise differences across the entire length of the two paralogs.

***SCN1A–SCN2A–SCN3A* coding sequences**

Species	Gene 1 – Gene 2	BC p-value	Protein begin	Protein end	P-loop	Exon	Length (bp)	Total poly (bp)	Num diffs (bp)	Total diffs (bp)
A. mexicanum	*SCN1A - SCN2A*	0.01	12	42	-	1	93	48	5	794
	SCN1A - SCN3A	0.01	45	84	-	1	128	54	5	722
	SCN2A - SCN3A	0.00	203	405	DI	5; 6; 7; 8 19; 20;	>626	74	2	902
	SCN1A - SCN2A	0.00	1059	1193	-	21	>407	134	25	794
	SCN1A - SCN3A	0.02	1104	1144	-	20	127	37	1	722
	***SCN1A - SCN2A*†**	**0.02**	**1208**	**1232**	**DIII**	**21**	**84**	**35**	**2**	**794**
C. alleganiensis	*SCN1A - SCN2A*	0.00	1111	1232	DIII	20;21	>376	153	23	621
	***SCN2A - SCN3A*†**	**0.02**	**1478**	**1611**	**DIV**	**26**	**406**	**164**	**32**	**693**
	SCN1A - SCN2A	0.00	1531	1652	DIV	26	371	177	27	621
N. viridescens	*SCN1A - SCN3A*	0.00	500	512	-	10	89	41	1	733
	SCN1A - SCN2A	0.01	1104	1199	-	16	292	109	20	796
P. cinereus	*SCN1A - SCN2A*	0.00	12	32	-	1	64	31	0	838
	SCN1A - SCN3A	0.00	362	499	DI	8; 9; 10	>576	88	13	786
	SCN2A - SCN3A	0.02	573	599	-	13	83	29	2	897
	SCN1A - SCN3A	0.00	610	667	-	14	177	68	8	786
						20; 21; 22; 23;				
	SCN1A - SCN2A	0.00	1135	1305	DIII	24	>524	138	9	838
	SCN1A - SCN3A	0.03	1430	1473	-	26	134	46	5	786
P. waltl	*SCN1A - SCN3A*	0.03	1369	1386	-	25	56	30	0	738
T. granulosa	***SCN1A - SCN3A****	**0.01**	**374**	**408**	**DI**	**8**	**105**	**41**	**2**	**725**
T. torosa	***SCN1A - SCN3A****	**0.01**	**374**	**408**	**DI**	**8**	**105**	**41**	**2**	**725**

***SCN4A* exon 26**

Species	Gene	BC p-value	Protein begin	Protein end	P-loop	Exon	Length (bp)	Total poly (bp)	Num diffs (bp)	Total diffs (bp)
P. cinereus	*SCN4A*	0.01	1509	1534	DIV	26a-26b	77	26	0	154
T. torosa	***SCN4A****	**0.02**	**1518**	**1536**	**DIV**	**26a-26b**	**56**	**22**	**1**	**178**

Discussion

Here we show that TTX-bearing newts have evolved resistance to their own toxicity through multiple parallel changes in their *SCNA* genes and that, similar to snakes that consume TTX-containing prey (McGlothlin et al. 2016; Perry et al. 2018), some of the resistance in this taxon is ancient, first appearing in an early salamander. However, while substitutions conferring moderate TTX resistance are present in some non-toxic salamander genomes, only the TTX-bearing newts have substitutions conferring high resistance across all six of their *SCNA* paralogs, and several of these channels harbor multiple resistant substitutions in more than one domain. Many of the substitutions conferring resistance to toxic newts are also present in *SCNA* paralogs of TTX-resistant pufferfish (Jost et al. 2008) and snakes (McGlothlin et al. 2016). Similar to pufferfish, newts appear to require resistance within all of their brain/nerve channels in addition to their hearts and muscles. This feature apparently distinguishes toxic prey from their predators, whose brain channels lack resistant substitutions (McGlothlin et al. 2014). This molecular parallelism emphasizes the strong structural and functional constraints on this gene family, which appear to limit the evolution of TTX resistance to a small number of predictable pathways, leading to convergent and parallel changes across multiple taxa (Feldman et al. 2012). We show that the evolution of extreme TTX resistance is accompanied by a shift in signatures of selection in four out of six paralogs, with suggestive evidence of positive selection acting directly on TTX-binding sites. Finally, the evolution of physiological resistance appears to have been facilitated by at least two instances of non-allelic gene conversion, which acted to introduce TTX-resistance substitutions from one paralog (or exon duplicate) to another.

Our reconstruction of the history of TTX resistance in salamanders reveals the ancient origins of moderate resistance in nerve channels $Na_v1.1$ and $Na_v1.6$ and high resistance in the heart channel $Na_v1.5$, which arose ~160 mya. Resistant substitutions in the muscle channel $Na_v1.4$ evolved later, becoming fixed in the clade including all newts and *S. salamandra* between 75–130 mya. This was followed by the accumulation of additional substitutions in DIII, DIVa, and DIVb of $Na_v1.4$ within members of the highly toxic newt clade, providing their muscles with resistance to much higher concentrations of TTX relative to salamanders lacking these mutations (Hanifin and Gilly 2015). Substitutions in DI conferring extreme TTX resistance to the brain/nerve channels $Na_v1.1$, $Na_v1.2$, $Na_v1.3$, and $Na_v1.6$ also evolved more recently (~37–50 mya) and they are limited to the toxic newt clade with only one exception, $Na_v1.1$ of *P. cinereus*,

379 which may have arisen independently in this lineage. Toxic newts also have unique substitutions
380 in DIV of $Na_v1.1$ and $Na_v1.2$, which may provide additional resistance to their brain channels or
381 may compensate for structural or functional changes resulting from resistant substitutions in DI
382 or in other regions of the protein. The widespread presence of TTX in modern newts suggests
383 that possession of TTX evolved in the common ancestor this clade (Hanifin 2010). This is
384 supported by our observation of shared TTX-resistance substitutions across all *SCNA* paralogs in
385 highly toxic newts. However, the highly toxic newts included in this study are limited to North
386 American species and do not include Asian or European newts (e.g. *Cynops* and *Triturus* spp.)
387 known to have TTX (Hanifin 2010). Sequencing the *SCNA*s of these species will reveal if
388 extreme resistance in the nerve channels is specific to North American newts or arose earlier in
389 an ancestral newt species.
390 Whether the TTX-resistance substitutions observed in newt relatives are adaptive and
391 what selective pressures act to retain them remains to be determined. In ancestral salamandrids,
392 resistance in three or four of the six *SCNA*s may have provided tolerance to low levels of TTX,
393 facilitating the evolution of extreme toxicity in the modern newts, although it is unclear whether
394 these substitutions arose in response to TTX exposure or as a side effect of selection for another
395 aspect of channel function. Environmental exposure to TTX could potentially occur from TTX-
396 bearing prey, such as terrestrial *Bipalium* flatworms (Stokes et al. 2014) or from TTX-producing
397 bacteria (Vaelli et al. 2020). In a feeding study on *B. adventitium* flatworms, Ducey et al. (1999)
398 demonstrated that while all salamanders rejected the flatworms when they were first presented,
399 some habituated *Ambystoma* and *Plethodon* individuals were able to consume them with only
400 minor symptoms of TTX poisoning, including apparent mucus production and numbing of the
401 mouth. Although the amount of TTX present in the worms was not measured, this observation
402 supports the conjecture that these substitutions play a protective role against consuming toxic
403 prey.
404 Our power to detect sites undergoing positive selection was low due to the small number
405 of species available for our analyses and the high sequence conservation among orthologs
406 (Anisimova et al. 2001; Yang et al. 2000). However, our analyses provided evidence consistent
407 with positive selection acting on TTX-binding sites, including sites implicated in the extreme
408 TTX resistance of salamander muscle fibers. Our branch models indicate that several Na_v
409 paralogs have higher ω ratios within the tetrodotoxic newt clade relative to other salamanders.

This increase in ω ratio appears to be mainly the result of relaxed purifying selection rather than positive selection, as few sites were estimated to have ω > 1 by branch-site models. Muscle channel $Na_v1.4$ had the highest ω ratio in toxic newts, coinciding with a relatively high proportion (~0.06) of sites detected as undergoing positive selection in toxic newts and purifying selection in other salamanders, although the likelihood ratio test was non-significant (Table S4). This pattern may derive from ongoing positive selection on *SCN4A* resulting from the coevolutionary arms race between newts and snakes. Increased ω ratios in toxic newts coincide with the appearance of highly TTX-resistant substitutions within the DI P-loops of $Na_v1.1$, $Na_v1.3$, and $Na_v1.6$, DIV of $Na_v1.1$, and the DIII, DIVa, and DIVb P-loops in $Na_v1.4$. While the pattern of these substitutions suggests that they are adaptive changes that occurred specifically within the tetrodotoxic newt clade, our branch-site models detected positive selection on TTX-binding sites only within the DIV P-loop of $Na_v1.1$ and the DIII and DIVa P-loops of $Na_v1.4$, while our site models detected positive selection on site 401 within paralogs $Na_v1.1$, $Na_v1.3$, and $Na_v1.6$ of all salamanders. This may be due to the statistically conservative nature of the branch-site model and the tendency of PAML to detect ongoing diversifying selection rather than rare positive selection events (Yang and dos Reis 2010). Furthermore, the site and branch-site models do not distinguish between biochemically conservative and non-conservative amino acid changes. Nevertheless, the detection of relatively high ω ratios within the toxic newt clade along with site-specific positive selection at known TTX-binding sites provides strong evidence that these substitutions are adaptive.

In addition to the six *SCNA* paralogs described in amphibians (Zakon 2012), our sequence data revealed the presence of a partial duplication of the *SCN4A* gene in salamanders that includes the entirety of exon 26, encoding the DIV P-loop, which likely occurred in an ancestor of Salamandroidea. The maintained open reading frame and shared expression patterns of transcripts encoding exons 26a and 26b in *A. mexicanum* tissues suggests that this duplicate region is functional in salamander muscles. In some insects that feed on toxic plants, the appearance of resistance-conferring substitutions is accompanied by one or more duplications of the genes that the toxin targets (Petschenka et al. 2017; Zhen et al. 2012). Petschenka et al. (2017) show that in at least one species, such gene duplication precedes resistance, and they suggest that gene duplication may help to alleviate the potential decrease in fitness incurred by the insects due to the negative pleiotropic effects of toxin-resistant mutations. Similarly,

441 resistance in DIV of salamander *SCN4A* appears after the duplication of this domain, and only
442 the TTX-bearing newts have resistant substitutions in both exon copies, lending support to this
443 hypothesis and raising the possibility that the evolution of physiological resistance in
444 salamanders may have been mediated in part by this genomic novelty.

445 We observed a rare case of the generation of adaptive variants via non-allelic gene
446 conversion, which occurred both between the duplicated exons of *SCN4A* and between paralogs
447 *SCN1A* and *SCN3A*. Gene conversion is often thought to play a role in constraint, preserving the
448 core functions of gene families (Chapman et al. 2006) and reducing deleterious mutation loads
449 (Khakhlova and Bock 2006; Ohta 1989), and has also been associated with the diversification of
450 major histocompatibility complex genes in mammals (Go et al. 2003; Kuhner et al. 1991) and the
451 introduction of deleterious nonsynonymous mutations into different parts of the genome (Casola
452 et al. 2012; Galtier et al. 2009). However, the potential for gene conversion to facilitate
453 adaptation is less widely appreciated. Theory suggests that gene duplication and subsequent gene
454 conversion may allow for movement between adaptive peaks via the accumulation of beneficial
455 mutations in one gene copy that can be transferred to a favorable genetic background (Hansen et
456 al. 2000). This process has been implicated in the adaptive evolution of hypoxia tolerance in
457 high-altitude Tibetan wolves (Signore et al. 2019) and in heavy metal tolerance in *Arabidopsis*
458 (Hanikenne et al. 2013). Here, we provide evidence that gene conversion contributed to the
459 spread of TTX-resistant amino acid substitutions. In the brain channel genes *SCN1A* and *SCN3A*,
460 this likely occurred between two genes that had previously evolved resistance, homogenizing the
461 substitutions between the two paralogs in *Taricha* newts. In the muscle channel gene *SCN4A*,
462 three identical amino acids were present within both duplicated DIV TTX-binding domains in
463 toxic newts, while only one resistant amino acid was present in a single DIV domain in their
464 non-tetrodotoxic salamander relatives, suggesting that resistant substitutions accumulated in one
465 exon copy in a toxic newt ancestor and subsequently spread to the other exon copy via gene
466 conversion. Both Hanifin and Gilly (2015) and Du et al. (2009) have shown that the single
467 resistant amino acid observed in less toxic salamanders confers only low levels of TTX
468 resistance, while the combination of the three amino acids found in highly toxic newts confers
469 extreme resistance. As splice variants encoding the alternative exons appear to share similar
470 expression patterns in salamanders, both exon copies should require extreme resistance in
471 species exposed to high TTX concentrations. The concerted evolution of TTX resistance among

homologous P-loop domains of *SCN4A* may have expedited the evolution of extreme resistance in newt muscles, requiring new resistant mutations to appear in only one of these domains before being transferred to the other copy.

The degree of parallel molecular evolution among members of the *SCNA* gene family and across lineages provides insight into the constraints on *SCNA* nucleotide sequence as well as the evolvability of the TTX-resistance phenotype. Our results reveal that similar to their coevolutionary partners, *Thamnophis* garter snakes, *Taricha* newts evolved extreme TTX resistance through a stepwise process that built upon ancient changes that were in place millions of years before the arms race began. However, the pattern of TTX resistance evolution in newts also displays important differences from that of their predators. First, perhaps because of the constitutive presence of TTX, newts display extreme levels of resistance even in channels that are expressed in the central nervous system, which are protected by the blood-brain barrier in species that encounter TTX in their diet. Second, our analysis indicates that many substitutions may have become fixed relatively close to one another in evolutionary time within the clade of modern newts. This is in contrast to snakes, where key changes were separated by millions of years. Due to our lack of sampling of newt species outside of North America, however, further work is necessary to understand the timing of these changes on a finer scale. We also show that while positive selection appears to be a strong driving force of the evolution of TTX auto-resistance in newts, gene conversion may have sped up the process of adaptive evolution in some *SCNA* paralogs, and constraints have limited the possible locations and types of resistant substitutions to a small subset of realized genetic changes. Taken together, our results emphasize the interplay among selection, constraint, and historical contingency in the evolution of complex adaptations.

Methods

Sequencing and annotation of voltage-gated sodium channel paralogs

We identified *SCNA* genes in the two publicly available salamander genome assemblies, *A. mexicanum* (Smith et al. 2019; AmexG.v6 assembly) and *P. waltl* (Elewa et al. 2017), and in one full-body transcriptome from the fire salamander *S. salamandra* (Goedbloed et al. 2017; BioProject accession PRJNA607429) using the reciprocal best BLAST hit method (Moreno-Hagelsieb and Latimer 2007) with queries of *SCNA* sequences from *X. tropicalis* (Hellsten et al. 2010) and salamanders (Hanifin and Gilly 2015). We confirmed assignments of each amphibian *SCNA* paralog based on nucleotide alignments of the coding sequences with *Xenopus* sequences, as well as synteny of the chromosomal segments containing *SCNA* genes (Fig. S1). These *SCNA* annotations were then used to design targeted sequencing probes and to subsequently assign paralog identity to our de novo salamander assemblies. We used Geneious v10.2.3 for sequence visualization and to create DNA and protein alignments (Kearse et al. 2012).

We also performed BLASTn searches of published transcriptome assemblies of *Tylototriton wenxianensis* (PRJNA323392), *Bolitoglossa vallecula* (PRJNA419601), and *Hynobius retardatus* (Matsunami et al. 2015; PRJDB2409). However, we were unable to identify the full set of *SCNA* paralogs within these three assemblies. Therefore, we used the sequences for probe design and to identify exon duplications in *SCN4A* but excluded them from PAML analyses.

In order to design targeted sequencing probes, we compiled partial and complete amphibian *SCNA* sequences obtained from NCBI databases and additional published sources (Table S8) into a single FASTA file. Each individual FASTA entry included a single exon and, when available, up to 200 bp of intron sequence upstream and downstream of each exon to aid in paralog assignment. Using RepeatMasker (Smit et al. 2013-2015), we replaced transposable elements and other sequence repeats with Ns, and subsequently filtered out sequences < 120 bp in length, as well as those with more than 25% missing or ambiguous characters. We submitted this masked and filtered file, which was 465 kb in total length, to Agilent Technologies (Santa Clara, CA, USA) for custom probe design using the SureSelect tool, resulting in 7518 unique 120-mer probes.

We obtained DNA samples from adult individuals of three TTX-bearing species (n=3 for each species): *T. torosa* from Hopland, CA, *T. granulosa* from Benton, OR, and *N. viridescens*

526 from Mountain Lake, VA, and from two additional salamander species presumed to lack TTX (*n*
527 = 2 for each species): *P. cinereus* collected in Mountain Lake, VA and *C. alleganiensis* collected
528 in southwestern VA. We extracted genomic DNA using the DNeasy Blood & Tissue kit (Qiagen
529 Inc., Valencia, CA) and prepared sequencing libraries using the SureSelect^{XT} Target Enrichment
530 system for Illumina paired-end multiplexed sequencing from Agilent Technologies (Santa Clara,
531 CA, USA), following the protocol for low input (200 ng) DNA samples. We used a Covaris
532 M220 Focused-ultrasonicator to shear 200 ng of purified whole genomic DNA from each sample
533 into ~250 bp fragments using the following settings: duty factor 10%, peak incident power 75 w,
534 200 cycles per burst, and treatment time of 160 seconds. We followed the Agilent SureSelect^{XT}
535 Target Enrichment kit protocol for end repair, adaptor ligation, amplification, hybridization and
536 bead capture (using the custom SureSelect probes described above), indexing, and purification.
537 We quantified the resulting enriched, indexed libraries with qPCR and combined them in
538 equimolar concentrations into one final library pool, which was submitted to the Genomics
539 Sequencing Center at Virginia Tech for sequencing on an Illumina MiSeq 300-cycle v2 with 150
540 bp paired-end reads. Prior to alignment, we trimmed Illumina reads of TruSeq3 adapter
541 sequences, removed bases with a phred64 quality score less than 3, and filtered out subsequent
542 reads shorter than 100 bp using Trimmomatic version 0.33 (Bolger et al. 2014). We used SPAdes
543 3.6.0 (Bankevich et al. 2012) to create de novo assemblies of the trimmed and filtered reads.
544 Each *SCNA* paralog had > 10-fold sequence coverage, with an average of 32-fold coverage
545 across all species and paralogs (Table S1).

546 Because we designed the sequencing probes to capture only small portions of the *SCNA*
547 intronic regions flanking exons (regions more likely to be conserved across species), each exon
548 was assembled into a separate scaffold. For each individual from our sequencing trial, we created
549 BLAST databases from the assembled de novo scaffolds and performed BLAST searches using
550 single exons from the *Ambystoma SCNA*s as queries. We created 26 separate nucleotide
551 alignments, one for each individual *SCNA* exon, including sequences from *Ambystoma*,
552 *Pleurodeles*, and our de novo assemblies using MAFFT v 7.450 (Katoh and Standley 2013) and
553 created consensus neighbor-joining trees with a Tamura-Nei genetic distance model using the
554 Geneious Tree Builder (Kearse et al. 2012) with 1000 bootstrap replicates and an 80% support
555 threshold. The resulting tree topologies were used to assign paralog identity to each of the exons.

When necessary, we included exon and intron sequences from additional species in the alignments to resolve the topology of the trees.

We concatenated all exons from each paralog into full coding sequences. Based on alignment with full-length *Xenopus* sequences, all salamander *SCNA* coding sequences collected for this study were >90% complete with the exception of two sequences from the *Salamandra salamandra* transcriptome (paralogs *SCN1A* and *SCN2A*, which were 68.8% and 70.7% complete respectively; Table S1). For each species, we used *SCNA* paralogs sequenced from the genome of a single individual for our downstream analyses, based on completeness of the assembly.

Determination TTX resistance levels

TTX sensitivity is commonly measured *in vitro* by using site-directed mutagenesis to introduce mutations of interest into a TTX-sensitive Na_v channel, followed by expression in *Xenopus* oocyte or HEK 293 cells and the application of patch-clamp whole-cell recordings to measure channel current in the presence of TTX. The fold-change in TTX sensitivity is then calculated by taking the ratio of the IC_{50} values, or the TTX concentration at which 50% of the Na_v channels are blocked, of mutated and wild-type channels (see Table 3 for references).

Another line of evidence for resistance in salamander muscle channels ($Na_v1.4$) comes from Hanifin and Gilly (2015), who estimated TTX sensitivity by recording action potentials generated from salamander muscle fibers and estimating the amount of TTX required to diminish the rise of the action potential, associating these relative changes with the presence and absence of substitutions in TTX-binding sites. They associated moderate TTX resistance (reduced sensitivity to 0.010 μM TTX) with the presence of DIII substitution M1240T and extreme resistance (low sensitivity to 300 μM TTX) with the presence of DIII and DIV substitutions M1240T, D1532S, and G1533D. We categorize levels of TTX resistance conferred by Na_v substitutions as extreme or moderate based on the results of Hanifin and Gilly (2015) as well as the data summarized in Table 3.

Phylogenetic analyses and identification of site-specific evolutionary rates

We constructed phylogenetic trees for the entire *SCNA* gene family using our *de novo* assembled sequences as well as sequences from the genomes of *A. mexicanum*, *P. waltl*, the whole-body transcriptome of *S. salamandra*, two frog genomes: *X. tropicalis* (Hellsten et al. 2010) and

Nanorana parkeri (Sun et al. 2015), and one fish genome: *Danio rerio* (Howe et al. 2013). We created an amino acid alignment of translated coding sequences using MAFFT v 7.450 (Katoh and Standley 2013) and constructed maximum likelihood trees from these alignments with RAxML v8.2.11 (Stamatakis 2014) in Geneious using a GAMMA BLOSSUM62 protein model and estimated clade support with 100 bootstrap replicates. In order to improve the accuracy of the nucleotide alignment, we used this amino acid alignments to guide codon alignments with PAL2NAL v14 (Suyama et al. 2006). We identified the best fitting substitution models for the nucleotide alignment using jModelTest 2.1.10 v20160303 (Darriba et al. 2012) and constructed maximum likelihood trees of the coding sequences with RAxML v8.2.11. The two models with the lowest AIC scores were (1) the transition model with unequal base frequencies, a gamma shape parameter, and some proportion of invariable sites (TIM2+I+G) and (2) a general time-reversible model with a gamma shape parameter and a proportion of invariable sites (GTR+I+G), which is nearly identical to TIM2+I+G, but includes two additional rate parameters (Posada 2008). Because the two models are nearly equivalent and both fit our data equally well, we chose the GTR+I+G model for its ease of implementation across different programs. We repeated these methods for each individual *SCNA* paralog for downstream analyses in PAML, excluding the sequences from the outgroup species *N. parkeri* and *D. rerio*.

We estimated synonymous (dS) and nonsynonymous (dN) substitution rates, as well as the d_N/d_S ratios (ω) for each paralog using codeml in PAML v4.8 (Yang 2007). In order to test for changes in selective regimes in the *SCNA* genes between salamanders and highly toxic newts (*Notophthalmus* and *Taricha* species), we fit the following models to our *SCNA* alignments: (1) one-ratio models (allowing for a single ω ratio among all sites and all branches of the phylogeny), (2) branch models (allowing for separate ω ratios for the foreground [toxic newts] and background [other salamanders]), (3) branch-site neutral models (allowing ω to vary both between toxic newts and other salamanders and among sites, with two possible categories: $0 < \omega < 1$ and $\omega = 1$), and (4) branch-site models (allowing ω to vary both between toxic newts and other salamanders and among sites, with three possible categories: $0 < \omega < 1$, $\omega = 1$, and $\omega > 1$, the latter being allowed only within toxic newts). To test for site-specific positive selection among all salamanders, we fit two sets of nested models: (1) discrete ω ratio models M1a vs. M2a, which allowing for ω to vary among sites, with either two possible categories: $0 < \omega < 1$ and $\omega = 1$ or three possible categories: $0 < \omega < 1$, $\omega = 1$, and $\omega > 1$; and (2) continuous ω ratio

models M7, M8a, and M8, which fit ω ratios of sites into a beta distribution, with ncatG (the number of ω values in the beta distribution) set to 5. We used F3x4 codon models, which estimate individual nucleotide frequencies for each of the three codon positions, and allowed codeml to estimate ω and transition-transversion rates (κ). The outputs of these models were used to estimate and compare gene-wide ω between toxic newts and salamanders (one-ratio and branch models), to identify sites under positive selection in all salamanders (site and neutral site models), and to identify sites under positive selection or with elevated ω in toxic newts relative to other salamanders (branch-site neutral and branch-site models). We also created ancestral sequence reconstructions by specifying RateAncestor = 1 within codeml configuration files for the neutral site models. We performed the above analyses both including and excluding the two *S. salamandra* paralogs with a large number of gaps (*SCN1A* and *SCN2A*). Maximum likelihood parameter estimates were largely congruent using these different datasets. Therefore, we present results from the gene trees including *S. salamandra* here.

Detection of gene conversion

We used the program GENECONV to detect potential nonallelic gene conversion events between *SCNA* paralogs. We used a full codon alignment of all six *SCNA* paralogs from 7 of the 8 salamanders included in the study (excluding *S. salamandra* due to missing data), but targeted our search to include only genes *SCN1A*, *SCN2A*, and *SCN3A* within each species under the assumption that gene conversion is more likely to occur between closely related sequences that reside on the same chromosome. This increased the power of detecting gene conversion from multiple pairwise comparisons. We also performed a separate search for gene conversion events between duplicate exons 26a and 26b of *SCN4A*. For this analysis, we used a codon alignment of *SCN4A* exons 26a and 26b from 10 salamander species. We assigned a mismatch penalty using gscale=1 and used Bonferroni-corrected *p*-values from 10,000 permutations to determine significance.

Acknowledgments

We thank Miguel Vences for helpful feedback on the manuscript and for providing an early draft of the *Salamandra salamandra* transcriptome. We also thank Vincent Farallo, Edmund Brodie III, William Hopkins, and Brian Case for providing DNA samples for this study, Kaitlyn Malewicz, Mercedes Collins, and Emily Orr for assistance with lab work, John Abramyan, Edmund Brodie III, Charles Hanifin, and Andrew Kern for helpful conversations and Matthew Hahn for advice on analyses and comments on the manuscript. Hellbender (*Cryptobranchus*) samples were collected by Brian Case and William Hopkins in cooperation with the Virginia Department of Wildlife Resources (DWR) and the U.S. Forest Service, and with assistance from J.D. Kleopfer. Hellbenders were handled under scientific collecting permit #060465 and approved Virginia Tech IACUC procedures (protocol #16-162). We thank the Departments of Fish and Wildlife in Oregon and California and the Virginia DWR for scientific collecting permits to MTJH (063-18, SC-11937 and 048104 respectively).

Article and author information

Author details

Kerry L Gendreau

ORCID: 0000-0001-6058-0893

- Department of Biological Sciences, Virginia Tech, Blacksburg, United States

Contribution: Performed experiments, formal analysis, investigation, visualization, methodology, writing – original draft, writing – review and editing.

Competing interests: No competing interests declared.

Angela D Hornsby

ORCID: 0000-0003-0927-2101

- Department of Biological Sciences, Virginia Tech, Blacksburg, United States
- Philip L. Wright Zoological Museum, Division of Biological Sciences, University of Montana, Missoula, United States

Contribution: Performed experiments, managed data, writing – review and editing.

Competing interests: No competing interests declared.

Michael TJ Hague

ORCID: 0000-0003-0641-2420

- Division of Biological Sciences, University of Montana, Missoula, MT, United States

Contribution: Collected samples, extracted and purified DNA, writing – review and editing.

Competing interests: No competing interests declared.

Joel W McGlothlin

ORCID: 0000-0003-3645-6264

- Department of Biological Sciences, Virginia Tech, Blacksburg, United States

Contribution: Conceptualization, investigation, formal analysis, writing – review and editing.

Competing interests: No competing interests declared.

Funding

National Science Foundation (DEB-1457463)

- Joel W McGlothlin

National Science Foundation (DEB-1601296)

- Michael TJ Hague

National Science Foundation (IOS-1755055)

- Joel W McGlothlin

Society for the Study of Evolution (R. C. Lewontin Award)

- Kerry L Gendreau

Virginia Tech Interfaces of Global Change (Graduate Fellowship Award)

- Kerry L Gendreau

Data availability

Newly generated sequences will be submitted to NCBI. Sequence alignments and configuration files for GENECONV analyses have been deposited at https://github.com/kerrygendreau/Newt-TTX-Resistance.git

References

Anisimova, M., J. P. Bielawski and Z. Yang. (2001). Accuracy and power of the likelihood ratio test in detecting adaptive molecular evolution. *Mol Biol Evol* 18 (8): 1585-1592. 10.1093/oxfordjournals.molbev.a003945

Arbuckle, K., R. C. Rodríguez de la Vega and N. R. Casewell. (2017). Coevolution takes the sting out of it: Evolutionary biology and mechanisms of toxin resistance in animals. *Toxicon* 140 118-131. 10.1016/j.toxicon.2017.10.026

Bankevich, A., S. Nurk, D. Antipov, A. A. Gurevich, M. Dvorkin, A. S. Kulikov*, et al.* (2012). SPAdes: A new genome assembly algorithm and its applications to single-cell sequencing. *J Comput Biol* 19 (5): 455-477. 10.1089/cmb.2012.0021

Bay, R. A. and J. P. Bielawski. (2011). Recombination detection under evolutionary scenarios relevant to functional divergence. *J Mol Evol* 73 (5-6): 273-286. 10.1007/s00239-011-9473-0

Benovoy, D. and G. Drouin. (2009). Ectopic gene conversions in the human genome. *Genomics* 93 (1): 27-32. 10.1016/j.ygeno.2008.09.007

Bolger, A. M., M. Lohse and B. Usadel. (2014). Trimmomatic: a flexible trimmer for Illumina sequence data. *Bioinformatics* 30 (15): 2114-2120. 10.1093/bioinformatics/btu170

Bricelj, V. M., L. Connell, K. Konoki, S. P. MacQuarrie, T. Scheuer, W. A. Catterall*, et al.* (2005). Sodium channel mutation leading to saxitoxin resistance in clams increases risk of PSP. *Nature* 434 (7034): 763-767. 10.1038/nature03415

Brodie, E. D., III and E. D. Brodie, Jr. (1990). Tetrodotoxin resistance in garter snakes: an evolutionary response of predators to dangerous prey. *Evolution* 44 (3): 651-659. 10.1111/j.1558-5646.1990.tb05945.x

Brodie, E. D., Jr., B. J. Ridenhour and E. D. Brodie, III. (2002). The evolutionary response of predators to dangerous prey: hotspots and coldspots in the geographic mosaic of coevolution between garter snakes and newts. *Evolution* 56 (10): 2067-2082. 10.1111/j.0014-3820.2002.tb00132.x

Bryant, D. M., K. Johnson, T. DiTommaso, T. Tickle, M. B. Couger, D. Payzin-Dogru*, et al.* (2017). A tissue-mapped axolotl de novo transcriptome enables identification of limb regeneration factors. *Cell Rep* 18 (3): 762-776. 10.1016/j.celrep.2016.12.063

Caballero-Pérez, J., A. Espinal-Centeno, F. Falcon, L. F. García-Ortega, E. Curiel-Quesada, A. Cruz-Hernández*, et al.* (2018). Transcriptional landscapes of Axolotl (*Ambystoma mexicanum)*. *Dev Biol* 433 (2): 227-239. 10.1016/j.ydbio.2017.08.022

738 Casola, C. and M. W. Hahn. (2009). Gene conversion among paralogs results in moderate false
739 detection of positive selection using likelihood methods. *J Mol Evol* 68 (6): 679-687.
740 10.1007/s00239-009-9241-6

741 Casola, C., U. Zekonyte, A. D. Phillips, D. N. Cooper and M. W. Hahn. (2012). Interlocus gene
742 conversion events introduce deleterious mutations into at least 1% of human genes
743 associated with inherited disease. *Genome Res* 22 (3): 429-435. 10.1101/gr.127738.111

744 Chapman, B. A., J. E. Bowers, F. A. Feltus and A. H. Paterson. (2006). Buffering of crucial
745 functions by paleologous duplicated genes may contribute cyclicality to angiosperm
746 genome duplication. *P Natl Acad Sci USA* 103 (8): 2730. 10.1073/pnas.0507782103

747 Chen, J.-M., D. N. Cooper, N. Chuzhanova, C. Férec and G. P. Patrinos. (2007). Gene
748 conversion: mechanisms, evolution and human disease. 8 (10): 762-775.
749 10.1038/nrg2193

750 Darriba, D., G. L. Taboada, R. Doallo and D. Posada. (2012). jModelTest 2: more models, new
751 heuristics and parallel computing. *Nat Methods* 9 (8): 772-772. 10.1038/nmeth.2109

752 Drouin, G. (2002). Characterization of the gene conversions between the multigene family
753 members of the yeast genome. *J Mol Evol* 55 (1): 14-23. 10.1007/s00239-001-0085-y

754 Du, Y., Y. Nomura, Z. Liu, Z. Y. Huang and K. Dong. (2009). Functional expression of an
755 arachnid sodium channel reveals residues responsible for tetrodotoxin resistance in
756 invertebrate sodium channels. *J Biol Chem* 284 (49): 33869-33875.
757 10.1074/jbc.M109.045690

758 Ducey, P. K., M. Messere, K. Lapoint and S. Noce. (1999). Lumbricid prey and potential
759 herpetofaunal predators of the invading terrestrial flatworm Bipalium adventitium
760 (Turbellaria: Tricladida: Terricola). *Am Midl Nat* 141 (2): 305-314. 10.1674/0003-
761 0031(1999)141[0305:LPAPHP]2.0.CO;2

762 Elewa, A., H. Wang, C. Talavera-López, A. Joven, G. Brito, A. Kumar*, et al.* (2017). Reading
763 and editing the Pleurodeles waltl genome reveals novel features of tetrapod regeneration.
764 *Nat Commun* 8 (1): 2286. 10.1038/s41467-017-01964-9

765 Feldman, C. R., E. D. Brodie, Jr., E. D. Brodie, III and M. E. Pfrender. (2012). Constraint shapes
766 convergence in tetrodotoxin-resistant sodium channels of snakes. *Proc Natl Acad Sci*
767 *USA* 109 (12): 4556-4561. 10.1073/pnas.1113468109

768 Fux, J. E., A. Mehta, J. Moffat and J. D. Spafford. (2018). Eukaryotic voltage-gated sodium
769 channels: on their origins, asymmetries, losses, diversification and adaptations. *Front*
770 *Physiol* 9 1406. 10.3389/fphys.2018.01406

771 Galtier, N., L. Duret, S. Glémin and V. Ranwez. (2009). GC-biased gene conversion promotes
772 the fixation of deleterious amino acid changes in primates. *Trends Genet* 25 (1): 1-5.
773 10.1016/j.tig.2008.10.011

774 Geffeney, S. L., E. D. Brodie, Jr., P. C. Ruben and E. D. Brodie, III. (2002). Mechanisms of
775 adaptation in a predator-prey arms race: TTX-resistant sodium channels. *Science* 297
776 (5585): 1336-1339. 10.1126/science.1074310

777 Geffeney, S. L., E. Fujimoto, E. D. Brodie, III, E. D. Brodie, Jr. and P. C. Ruben. (2005).
778 Evolutionary diversification of TTX-resistant sodium channels in a predator-prey
779 interaction. *Nature* 434 (7034): 759-763. 10.1038/nature03444

780 Go, Y., Y. Satta, Y. Kawamoto, G. Rakotoarisoa, A. Randrianjafy, N. Koyama*, et al.* (2003).
781 Frequent segmental sequence exchanges and rapid gene duplication characterize the
782 MHC class I genes in lemurs. *Immunogenetics* 55 (7): 450-461. 10.1007/s00251-003-
783 0613-6

784 Goedbloed, D. J., T. Czypionka, J. Altmüller, A. Rodriguez, E. Küpfer, O. Segev*, et al.* (2017).
785 Parallel habitat acclimatization is realized by the expression of different genes in two
786 closely related salamander species (genus *Salamandra*). *Heredity* 119 (6): 429-437.
787 10.1038/hdy.2017.55

788 Graham, A. M. and K. G. McCracken. (2019). Convergent evolution on the hypoxia-inducible
789 factor (HIF) pathway genes EGLN1 and EPAS1 in high-altitude ducks. *Heredity* 122 (6):
790 819-832. 10.1038/s41437-018-0173-z

791 Hague, M. T. J., A. N. Stokes, C. R. Feldman, E. D. Brodie Jr. and E. D. Brodie III. (2020). The
792 geographic mosaic of arms race coevolution is closely matched to prey population
793 structure. *Evol Lett* 4 (4): 317-332. 10.1002/evl3.184

794 Hanifin, C. T. (2010). The chemical and evolutionary ecology of tetrodotoxin (TTX) toxicity in
795 terrestrial vertebrates. *Mar Drugs* 8 (3): 577-593. 10.3390/Md8030577

796 Hanifin, C. T. and W. F. Gilly. (2015). Evolutionary history of a complex adaptation:
797 tetrodotoxin resistance in salamanders. *Evolution* 69 (1): 232-244. 10.1111/evo.12552

798 Hanikenne, M., J. Kroymann, A. Trampczynska, M. Bernal, P. Motte, S. Clemens*, et al.* (2013).
799 Hard selective sweep and ectopic gene conversion in a gene cluster affording
800 environmental adaptation. *PLOS Genet* 9 (8): e1003707. 10.1371/journal.pgen.1003707

801 Hansen, T. F., A. J. R. Carter and C.-H. Chiu. (2000). Gene conversion may aid adaptive peak
802 shifts. *J Theor Biol* 207 (4): 495-511. 10.1006/jtbi.2000.2189

803 Hellsten, U., R. M. Harland, M. J. Gilchrist, D. Hendrix, J. Jurka, V. Kapitonov*, et al.* (2010).
804 The genome of the western clawed frog *Xenopus tropicalis*. *Science* 328 (5978): 633-636.
805 10.1126/science.1183670

806 Hime, P. M., A. R. Lemmon, E. C. M. Lemmon, E. Prendini, J. M. Brown, R. C. Thomson*, et al.*
807 (2021). Phylogenomics reveals ancient gene tree discordance in the amphibian tree of
808 life. *Syst Biol* 70 (1): 49-66. 10.1093/sysbio/syaa034

Howe, K., M. D. Clark, C. F. Torroja, J. Torrance, C. Berthelot, M. Muffato*, et al.* (2013). The zebrafish reference genome sequence and its relationship to the human genome. *Nature* 496 (7446): 498-503. 10.1038/nature12111

Jeziorski, M. C., R. M. Greenberg and P. A. V. Anderson. (1997). Cloning of a putative voltage-gated sodium channel from the turbellarian flatworm *Bdelloura candida*. *Parasitology* 115 (3): 289-296. 10.1017/S0031182097001388

Jost, M. C., D. M. Hillis, Y. Lu, J. W. Kyle, H. A. Fozzard and H. H. Zakon. (2008). Toxin-resistant sodium channels: parallel adaptive evolution across a complete gene family. *Mol Biol Evol* 25 (6): 1016-1024. DOI 10.1093/molbev/msn025

Katoh, K. and D. M. Standley. (2013). MAFFT multiple sequence alignment software version 7: improvements in performance and usability. *Mol Biol Evol* 30 (4): 772-780. 10.1093/molbev/mst010

Kearse, M., R. Moir, A. Wilson, S. Stones-Havas, M. Cheung, S. Sturrock*, et al.* (2012). Geneious Basic: An integrated and extendable desktop software platform for the organization and analysis of sequence data. *Bioinformatics* 28 (12): 1647-1649. 10.1093/bioinformatics/bts199

Khakhlova, O. and R. Bock. (2006). Elimination of deleterious mutations in plastid genomes by gene conversion. *Plant J* 46 (1): 85-94. 10.1111/j.1365-313X.2006.02673.x

Kosakovsky Pond, S. L. and S. D. W. Frost. (2005). Not so different after all: a comparison of methods for detecting amino acid sites under selection. *Mol Biol Evol* 22 (5): 1208-1222. 10.1093/molbev/msi105

Kuhner, M. K., D. A. Lawlor, P. D. Ennis and P. Parham. (1991). Gene conversion in the evolution of the human and chimpanzee MHC class I loci. *Tissue Antigens* 38 (4): 152-64. 10.1111/j.1399-0039.1991.tb01889.x

Leffler, A., R. I. Herzog, S. D. Dib-Hajj, S. G. Waxman and T. R. Cummins. (2005). Pharmacological properties of neuronal TTX-resistant sodium channels and the role of a critical serine pore residue. *Pflug Arch Eur J Phy* 451 (3): 454-463. 10.1007/s00424-005-1463-x

Losos, J. B. (2011). Convergence, adaptation, and constraint. *Evolution* 65 (7): 1827-1840. 10.1111/j.1558-5646.2011.01289.x

Márquez, R., V. Ramírez-Castañeda and A. Amézquita. (2019). Does batrachotoxin autoresistance coevolve with toxicity in *Phyllobates* poison-dart frogs? *Evolution* 73 (2): 390-400. 10.1111/evo.13672

Maruta, S., K. Yamaoka and M. Yotsu-Yamashita. (2008). Two critical residues in P-loop regions of pufferfish Na^+ channels on TTX sensitivity. *Toxicon* 51 (3): 381-387. 10.1016/j.toxicon.2007.10.014

Matsunami, M., J. Kitano, O. Kishida, H. Michimae, T. Miura and K. Nishimura. (2015). Transcriptome analysis of predator- and prey-induced phenotypic plasticity in the Hokkaido salamander (*Hynobius retardatus*). *Mol Ecol* 24 (12): 3064-3076. 10.1111/mec.13228

McGlothlin, J. W., J. P. Chuckalovcak, D. E. Janes, S. V. Edwards, C. R. Feldman, E. D. Brodie, Jr.*, et al.* (2014). Parallel evolution of tetrodotoxin resistance in three voltage-gated sodium channel genes in *Thamnophis sirtalis*. *Mol Biol Evol* 31 (11): 2386-2846. 10.1093/molbev/msu237

McGlothlin, J. W., M. E. Kobiela, C. R. Feldman, T. A. Castoe, F. J. Vonk, M. K. Richardson*, et al.* (2016). Historical contingency in a multigene family facilitates adaptive evolution of toxin resistance. *Curr Biol* 26 1616-1621. 10.1016/j.cub.2016.04.056

McGrath, C. L., C. Casola and M. W. Hahn. (2009). Minimal effect of ectopic gene conversion among recent duplicates in four mammalian genomes. *Genetics* 182 (2): 615-622. 10.1534/genetics.109.101428

Moreno-Hagelsieb, G. and K. Latimer. (2007). Choosing BLAST options for better detection of orthologs as reciprocal best hits. *Bioinformatics* 24 (3): 319-324. 10.1093/bioinformatics/btm585

Nowoshilow, S., S. Schloissnig, J.-F. Fei, A. Dahl, A. W. C. Pang, M. Pippel*, et al.* (2018). The axolotl genome and the evolution of key tissue formation regulators. *Nature* 554 (7690): 50-55. 10.1038/nature25458

Ohta, T. (1989). The mutational load of a multigene family with uniform members. *Genet Res* 53 (2): 141-145. 10.1017/S0016672300028020

Perry, B. W., D. C. Card, J. W. McGlothlin, G. I. M. Pasquesi, R. H. Adams, D. R. Schield*, et al.* (2018). Molecular adaptations for sensing and securing prey and insight into amniote genome diversity from the garter snake genome. *Genome Biol Evol* 10 (8): 2110-2129. 10.1093/gbe/evy157

Petschenka, G., V. Wagschal, M. von Tschirnhaus, A. Donath and S. Dobler. (2017). Convergently evolved toxic secondary metabolites in plants drive the parallel molecular evolution of insect resistance. *Am Nat* 190 (S1): S29-S43. 10.1086/691711

Posada, D. (2008). jModelTest: Phylogenetic model averaging. *Mol Biol Evol* 25 (7): 1253-1256. 10.1093/molbev/msn083

Posada, D. and K. A. Crandall. (2001). Evaluation of methods for detecting recombination from DNA sequences: computer simulations. *P Natl Acad Sci USA* 98 (24): 13757-13762. 10.1073/pnas.241370698

Rodríguez, A., J. D. Burgon, M. Lyra, I. Irisarri, D. Baurain, L. Blaustein*, et al.* (2017). Inferring the shallow phylogeny of true salamanders (*Salamandra*) by multiple phylogenomic approaches. *Mol Phylogenet Evol* 115 16-26. 10.1016/j.ympev.2017.07.009

882 Sawyer, S. A. (1999). GENECONV: a computer package for the statistical detection of gene
883 conversion. http://www.math.wustl.edu/~sawyer.

884 Semple, C. and K. H. Wolfe. (1999). Gene duplication and gene conversion in the
885 Caenorhabditis elegans genome. *J Mol Evol* 48 (5): 555-564. 10.1007/pl00006498

886 Signore, A. V., Y.-Z. Yang, Q.-Y. Yang, G. Qin, H. Moriyama, R.-L. Ge*, et al.* (2019). Adaptive
887 changes in hemoglobin function in high-altitude Tibetan canids were derived via gene
888 conversion and introgression. *Mol Biol Evol* 36 (10): 2227-2237.
889 10.1093/molbev/msz097

890 Smit, A., R. Hubley and P. Green. (2013-2015). RepeatMasker Open-4.0. Retrieved from
891 http://www.repeatmasker.org

892 Smith, J. J., N. Timoshevskaya, V. A. Timoshevskiy, M. C. Keinath, D. Hardy and S. R. Voss.
893 (2019). A chromosome-scale assembly of the axolotl genome. *Genome Res* 29 (2): 317-
894 324. 10.1101/gr.241901.118

895 Smith, S. D., M. W. Pennell, C. W. Dunn and S. V. Edwards. (2020). Phylogenetics is the new
896 genetics (for most of biodiversity). *Trends Ecol Evol* 35 (5): 415-425.
897 10.1016/j.tree.2020.01.005

898 Soong, T. W. and B. Venkatesh. (2006). Adaptive evolution of tetrodotoxin resistance in
899 animals. *Trends Genet* 22 (11): 621-626. DOI 10.1016/j.tig.2006.08.010

900 Stamatakis, A. (2014). RAxML version 8: a tool for phylogenetic analysis and post-analysis of
901 large phylogenies. *Bioinformatics* 30 (9): 1312-1313. 10.1093/bioinformatics/btu033

902 Stokes, A. N., P. K. Ducey, L. Neuman-Lee, C. T. Hanifin, S. S. French, M. E. Pfrender*, et al.*
903 (2014). Confirmation and distribution of tetrodotoxin for the first time in terrestrial
904 Invertebrates: two terrestrial flatworm species (*Bipalium adventitium* and *Bipalium*
905 *kewense*). *PLOS One* 9 (6): e100718. 10.1371/journal.pone.0100718

906 Storz, J. F. (2016). Causes of molecular convergence and parallelism in protein evolution. *Nat*
907 *Rev Genet* 17 (4): 239-250. 10.1038/nrg.2016.11

908 Sun, Y. B., Z. J. Xiong, X. Y. Xiang, S. P. Liu, W. W. Zhou, X. L. Tu*, et al.* (2015). Whole-
909 genome sequence of the Tibetan frog *Nanorana parkeri* and the comparative evolution of
910 tetrapod genomes. *P Natl Acad Sci USA* 112 (11): E1257. 10.1073/pnas.1501764112

911 Sunami, A., I. W. Glaaser and H. A. Fozzard. (2000). A critical residue for isoform difference in
912 tetrodotoxin affinity is a molecular determinant of the external access path for local
913 anesthetics in the cardiac sodium channel. *P Natl Acad Sci USA* 97 (5): 2326-2331.
914 10.1073/pnas.030438797

915 Suyama, M., D. Torrents and P. Bork. (2006). PAL2NAL: robust conversion of protein sequence
916 alignments into the corresponding codon alignments. *Nucleic Acids Res* 34 (Web Server
917 issue): W609-W612. 10.1093/nar/gkl315

Tarvin, R. D., C. M. Borghese, W. Sachs, J. C. Santos, Y. Lu, L. A. O'Connell*, et al.* (2017). Interacting amino acid replacements allow poison frogs to evolve epibatidine resistance. *Science* 357 (6357): 1261-1266. 10.1126/science.aan5061

Vaelli, P. M., K. R. Theis, J. E. Williams, L. A. O'Connell, J. A. Foster and H. L. Eisthen. (2020). The skin microbiome facilitates adaptive tetrodotoxin production in poisonous newts. *eLife* 9 e53898. 10.7554/eLife.53898

Venkat, A., M. W. Hahn and J. W. Thornton. (2018). Multinucleotide mutations cause false inferences of lineage-specific positive selection. *Nat Ecol Evol* 2 (8): 1280-1288. 10.1038/s41559-018-0584-5

Venkatesh, B., S. Q. Lu, N. Dandona, S. L. See, S. Brenner and T. W. Soong. (2005). Genetic basis of tetrodotoxin resistance in pufferfishes. *Curr Biol* 15 (22): 2069-2072. 10.1016/j.cub.2005.10.068

Widmark, J., G. Sundström, D. Ocampo Daza and D. Larhammar. (2011). Differential evolution of voltage-gated sodium channels in tetrapods and teleost fishes. *Mol Biol Evol* 28 (1): 859-871. 10.1093/molbev/msq257

Williams, B. L., C. T. Hanifin, E. D. Brodie, Jr. and E. D. Brodie, III. (2010). Tetrodotoxin affects survival probability of rough-skinned newts (*Taricha granulosa*) faced with TTX-resistant garter snake predators (*Thamnophis sirtalis*). *Chemoecology* 20 (4): 285-290. DOI 10.1007/s00049-010-0057-z

Yang, Z. (1998). Likelihood ratio tests for detecting positive selection and application to primate lysozyme evolution. *Mol Biol Evol* 15 (5): 568-573. 10.1093/oxfordjournals.molbev.a025957

Yang, Z. and M. dos Reis. (2010). Statistical properties of the branch-site test of positive selection. *Mol Biol Evol* 28 (3): 1217-1228. 10.1093/molbev/msq303

Yang, Z., R. Nielsen, N. Goldman and A.-M. K. Pedersen. (2000). Codon-substitution models for heterogeneous selection pressure at amino acid sites. *Genetics* 155 (1): 431-449.

Yang, Z., W. S. W. Wong and R. Nielsen. (2005). Bayes empirical Bayes inference of amino acid sites under positive selection. *Mol Biol Evol* 22 (4): 1107-1118. 10.1093/molbev/msi097

Yang, Z. H. (2007). PAML 4: Phylogenetic analysis by maximum likelihood. *Mol Biol Evol* 24 (8): 1586-1591. DOI 10.1093/molbev/msm088

Yu, F. H. and W. A. Catterall. (2003). Overview of the voltage-gated sodium channel family. *Genome Biol* 4 (3): 207. 10.1186/gb-2003-4-3-207

Zakon, H. H. (2012). Adaptive evolution of voltage-gated sodium channels: The first 800 million years. *P Natl Acad Sci USA* 109 (Supplement 1): 10619-10625. DOI 10.1073/pnas.1201884109

954 Zakon, H. H., M. C. Jost and Y. Lu. (2011). Expansion of voltage-dependent Na^+ channel gene
955 family in early tetrapods coincided with the emergence of terrestriality and increased
956 brain complexity. *Mol Biol Evol* 28 (4): 1415-1424. DOI 10.1093/molbev/msq325

957 Zhang, J., R. Nielsen and Z. Yang. (2005). Evaluation of an improved branch-site likelihood
958 method for detecting positive selection at the molecular level. *Mol Biol Evol* 22 (12):
959 2472-2479. 10.1093/molbev/msi237

960 Zhen, Y., M. L. Aardema, E. M. Medina, M. Schumer and P. Andolfatto. (2012). Parallel
961 molecular evolution in an herbivore community. *Science* 337 (6102): 1634-1637.
962 10.1126/science.1226630
963

Supporting information

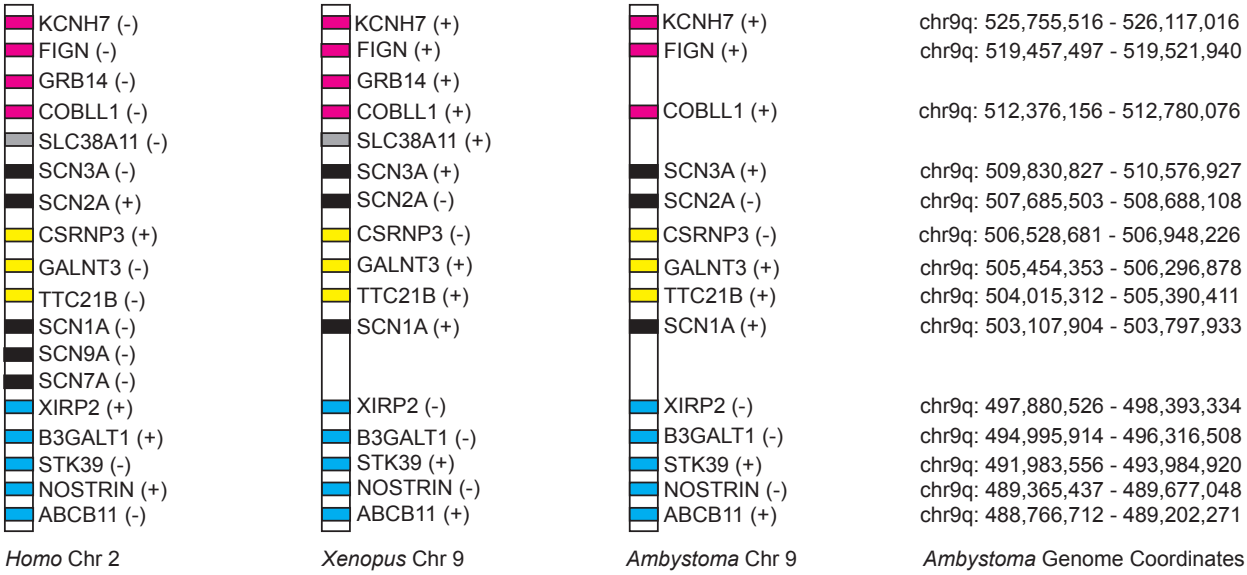

Figure S1. Conserved synteny of voltage-gated sodium channel paralogs across tetrapods. The genetic configuration of brain/nerve voltage-gated sodium channels (*SCNA* genes) is highly conserved across three tetrapod species: humans (*Homo*), frogs (*Xenopus*), and salamanders (*Ambystoma*). Genome coordinates are based on the AmexG.v6 assembly. Symbols (+) and (-) refer to gene orientation within this reference genome.

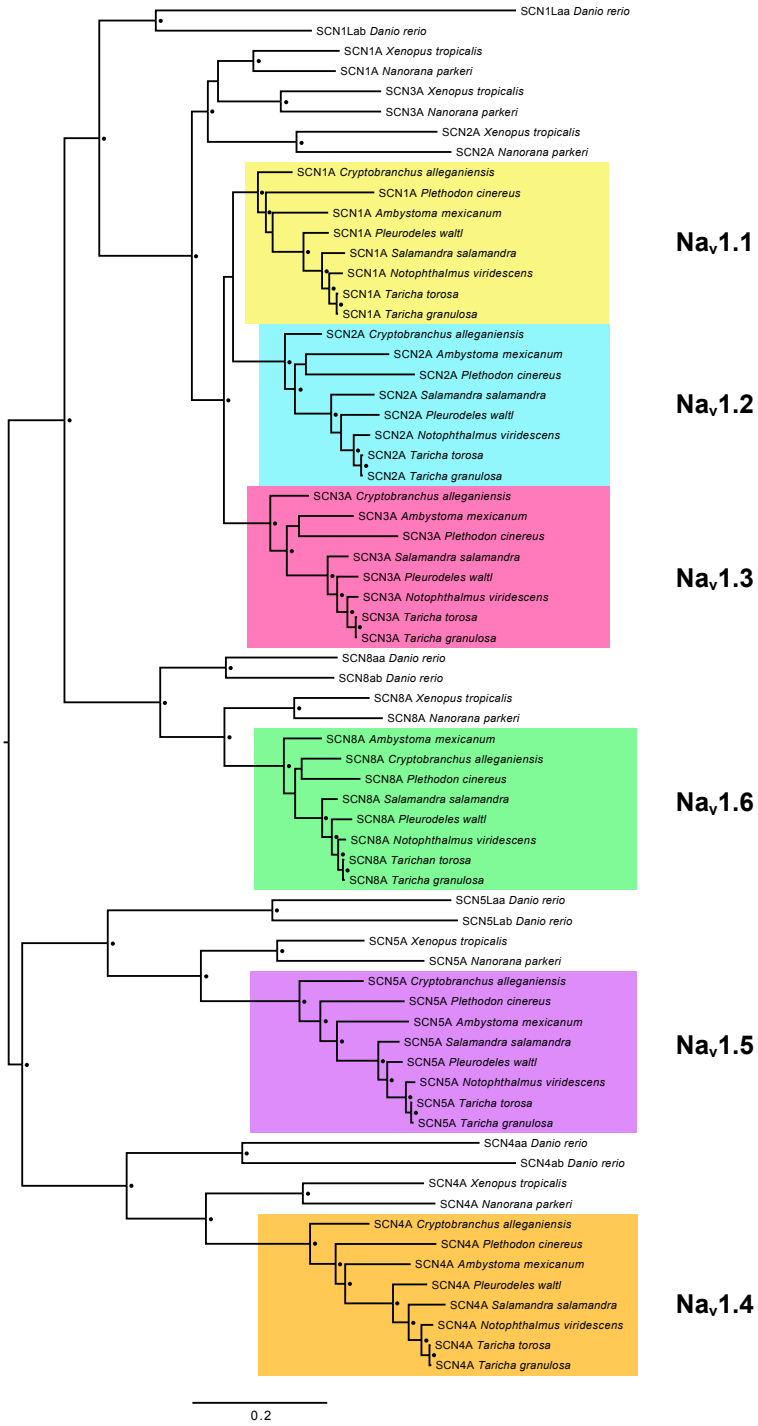

Figure S2. Maximum likelihood tree constructed from 6789 bp coding sequence alignment of salamander *SCNA* gene coding sequences with sequences from frogs (*Nanorana parkeri* and *Xenopus tropicalis*) and fish (*Danio rerio*) as outgroups. Black circles indicate nodes with bootstrap support >90%.

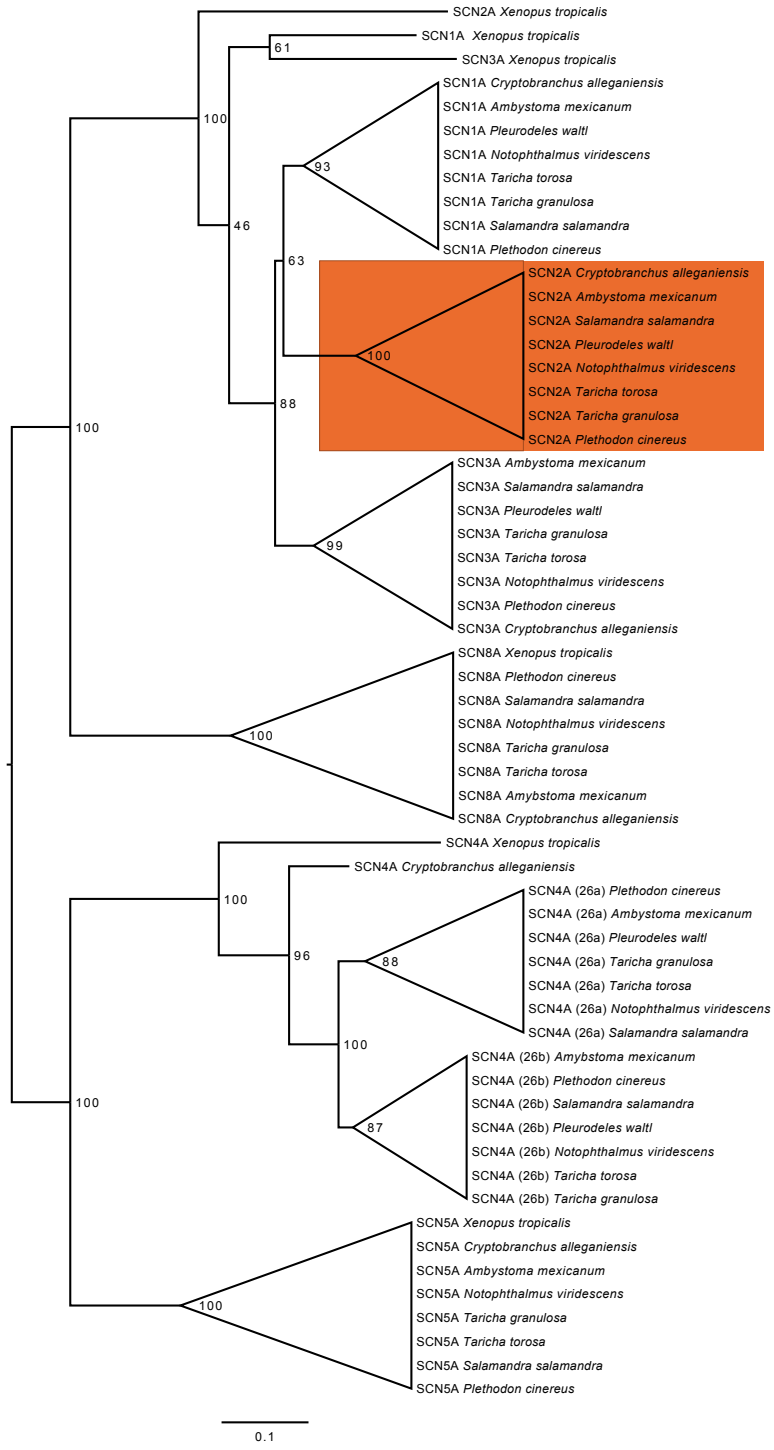

Figure S3. Maximum likelihood tree constructed from 1063 bp nucleotide alignment of *SCNA* exon 26 sequences. Node labels indicate bootstrap support from 100 replicates. Orange highlighting indicates clade grouping *SCN2A* from *Ambystoma* and other salamander species (bootstrap support 100%).

Table S1. Summary statistics from salamander *SCNA* sequencing and alignments. For each sequence, percent complete is calculated from the number of base pairs in a sequence divided by the total alignment length and pairwise percent identity is calculated from the average of all pairwise comparisons within an alignment. Average coverage is reported for all paralogs sequenced *de novo* in this study; sequences with unreported coverage were obtained from already published assemblies.

SCN1A ($Na_v1.1$)	**GC %**	**Length**	**Gaps**	**% Gaps**	**% Complete**	**Pairwise % identity**	**Average coverage**
Ambystoma mexicanum	42.3	6224	165	2.7	97.3	81.8	-
Pleurodeles waltl	42.0	6149	390	6.3	93.7	81.9	-
Cryptobranchus alleganiensis	42.5	6216	162	2.6	97.4	81.6	21.44
Notophthalmus viridescens	41.5	6188	231	3.7	96.3	84.3	21.33
Taricha granulosa	41.5	6224	201	3.2	96.8	85.2	42.41
Taricha torosa	41.4	6224	159	2.6	97.4	85.4	39.88
Salamandra salamandra	41.6	5915	1846	31.2	68.8	60.2	-
Plethodon cinereus	46.1	6219	477	7.7	92.3	75.1	13.42
Xenopus tropicalis	41.2	6216	153	2.5	97.5	73.4	-
SCN2A ($Na_v1.2$)	**GC %**	**Length**	**Gaps**	**% Gaps**	**% Complete**	**Pairwise % Identity**	**Average coverage**
Ambystoma mexicanum	43.5	5946	402	6.8	93.2	70.9	-
Pleurodeles waltl	41.5	5982	108	1.8	98.2	79.7	-
Cryptobranchus alleganiensis	41.3	6000	438	7.3	92.7	74.9	18.6
Notophthalmus viridescens	42.3	6039	432	7.2	92.8	13.4	22.54
Taricha granulosa	41.8	6060	75	1.2	98.8	81.7	40.43
Taricha torosa	41.9	6060	69	1.1	98.9	81.6	34.32
Salamandra salamandra	41.9	3672	1077	29.3	70.7	56.8	-
Plethodon cinereus	46.7	6006	700	10	90.0	68.4	22.7
Xenopus tropicalis	41.4	6054	141	2.3	97.7	66.4	-
SCN3A ($Na_v1.3$)	**GC %**	**Length**	**Gaps**	**% Gaps**	**% Complete**	**Pairwise % Identity**	**Average coverage**
Ambystoma mexicanum	45	6072	51	0.8	99.2	83.3	-
Pleurodeles waltl	42.3	6069	195	3.2	96.8	85.9	-
Cryptobranchus alleganiensis	43.3	6093	39	0.6	99.4	83.7	23.59
Notophthalmus viridescens	42.4	6078	72	1.2	98.8	88.3	49.48
Taricha granulosa	42.3	6093	72	1.2	98.8	88.6	42.71
Taricha torosa	42.2	6099	72	1.2	98.8	88.6	40.9
Salamandra salamandra	42.9	6096	186	3.1	96.9	85.3	-
Plethodon cinereus	47.9	6096	510	8.4	91.6	75.1	14.44
Xenopus tropicalis	42.2	6093	36	0.6	99.4	75.5	-
SCN4A ($Na_v1.4$)	**GC %**	**Length**	**Gaps**	**% Gaps**	**% Complete**	**Pairwise % Identity**	**Average coverage**
Ambystoma mexicanum	43.4	5034	141	2.8	97.2	81.8	-
Pleurodeles waltl	43.3	5622	96	1.7	98.3	85.3	-
Cryptobranchus alleganiensis	46.2	5580	48	0.9	99.1	80.9	12.46
Notophthalmus viridescens	43.6	5622	96	1.7	98.3	87.1	47.29
Taricha granulosa	44	5469	87	1.6	98.4	87.3	35.46
Taricha torosa	44	5469	90	1.6	98.4	87.4	42.97
Salamandra salamandra	44.5	5619	135	2.4	97.6	85.4	-
Plethodon cinereus	43.5	5628	279	5	95	78.2	12.2
Xenopus tropicalis	43.3	5622	111	2	98	71.2	-
SCN5A ($Na_v1.5$)	**GC %**	**Length**	**Gaps**	**% Gaps**	**% Complete**	**Pairwise % Identity**	**Average coverage**
Ambystoma mexicanum	48.9	5988	45	0.8	99.2	82.7	-
Pleurodeles waltl	44.7	5706	102	1.8	98.2	86.9	-
Cryptobranchus alleganiensis	47	5961	33	0.6	99.4	81.6	16.06
Notophthalmus viridescens	45.5	5943	42	0.7	99.3	88.6	55.83
Taricha granulosa	45.7	5967	42	0.7	99.3	88.8	58.51
Taricha torosa	45.7	5967	42	0.7	99.3	89.0	36.8
Salamandra salamandra	45.7	5097	237	4.6	95.4	84.1	-

Plethodon cinereus	48.7	5961	48	0.8	99.2	81.8	22.49
Xenopus tropicalis	47	5988	45	0.8	99.2	73.3	-
SCN8A (Na$_v$1.6)	**GC %**	**Length**	**Gaps**	**% Gaps**	**% Complete**	**Pairwise % Identity**	**Average coverage**
Ambystoma mexicanum	44.5	5946	30	0.5	99.5	88.0	-
Pleurodeles waltl	44.5	5691	84	1.5	98.5	90.0	-
Cryptobranchus alleganiensis	44.7	5946	21	0.4	99.6	88.2	21.26
Notophthalmus viridescens	44.7	5916	30	0.5	99.5	91.5	49.65
Taricha granulosa	44.8	5952	30	0.5	99.5	91.7	43.78
Taricha torosa	44.8	5907	30	0.5	99.5	91.8	35.75
Salamandra salamandra	44.9	5946	30	0.5	99.5	90.8	-
Plethodon cinereus	44.7	5949	42	0.7	99.3	86.8	32.32
Xenopus tropicalis	41.9	5946	18	0.3	99.7	79.1	-

Table S2. Synonymous and nonsynonymous polymorphism in salamander *SCNA* sequences obtained for this study using targeted sequence capture.

	SCN1A	*SCN2A*	*SCN3A*	*SCN4A*	*SCN5A*	*SCN8A*
***C. alleganiensis* (n=2)**						
Synonymous (P_s)	3	4	1	1	2	0
Nonsynonymous (P_n)	0	2	0	0	0	0
Insertions	0	0	0	0	0	0
Missing exons	0	1	0	0	0	0
***P. cinereus* (n=2)**						
Synonymous (P_s)	0	3	3	6	4	0
Nonsynonymous (P_n)	1	0	0	1	0	0
Insertions	0	0	0	0	0	0
Missing exons	0	2	2	1	0	0
***N. viridescens* (n=3)**						
Synonymous (P_s)	24	22	35	19	11	12
Nonsynonymous (P_n)	5	2	4	8	1	1
Insertions	1 (39 bases)	0	0	0	0	0
Missing exons	0	2	0	0	0	0
***T. torosa* (n=3)**						
Synonymous (P_s)	2	5	2	2	1	0
Nonsynonymous (P_n)	1	2	0	1	1	0
Insertions	0	0	0	1 (3 bases)	0	0
Missing exons	0	2	0	0	0	0
***T. granulosa* (n=3)**						
Synonymous (P_s)	4	8	3	10	4	5
Nonsynonymous (P_n)	0	0	0	2	2	0
Insertions	0	0	0	0	0	0
Missing exons	0	2	0	0	0	0

Table S3. Likelihood ratio tests from codeml site models. Included for each paralog are summaries of likelihood-ratio tests ($2\Delta\ell$) for site models using codeml from the PAML software program. Significance is indicated for p-values < 0.05 (*) and <0.01 (**) with critical values determined from the χ^2 distribution.

	ℓ	n Parameters	Parameter Estimates	$2\Delta\ell$
***SCN1A* ($Na_v1.1$)**				
Nearly neutral site model (M1a)	-20237.40	18	$p_0 = 0.91$, ($p_1 = 0.09$) $\omega_0 = 0.03$, ($\omega_1 = 1.00$)	-
Site selection model (M2a)	-20237.40	20	$p_0 = 0.91$, $p_1 = 0.09$, ($p_2 = 0.00$) $\omega_0 = 0.03$, ($\omega_1 = 1.00$), $\omega_2 = 50.8$	(M2a vs. M1a) **0.00**
Site null model (M7)	-20200.36	18	$p = 0.11$, $q = 1.01$	-
Site neutral model (M8a)	-20193.38	19	$p = 0.13$, $q = 1.69$	-
Site selection model (M8)	-20193.38	20	$p_0 = 0.96$, ($p_1 = 0.04$) $p = 0.13$, $q = 1.69$ $p_0 = 0.96$, ($p_1 = 0.04$), $\omega_1 = 1.00$	(M7 vs. M8) **13.97**** (M8 vs. M8a) **0.00**
***SCN2A* ($Na_v1.2$)**				
Nearly neutral site model (M1a)	-21559.11	18	$p_0 = 0.89$, ($p_1 = 0.11$) $\omega_0 = 0.05$, ($\omega_1 = 1.00$)	-
Site selection model (M2a)	-21559.11	20	$p_0 = 0.89$, $p_1 = 0.11$, ($p_2 = 0.00$) $\omega_0 = 0.05$, ($\omega_1 = 1.00$), $\omega_2 = 45.2$	(M2a vs. M1a) **0.00**
Site null model (M7)	-21481.17	18	$p = 0.19$, $q = 1.43$	-
Site neutral model (M8a)	-21474.94	19	$p = 0.22$, $q = 2.14$	-
Site selection model (M8)	-21474.89	20	$p_0 = 0.97$, ($p_1 = 0.03$) $p = 0.21$, $q = 2.07$ $p_0 = 0.98$, ($p_1 = 0.02$), $\omega_1 = 1.09$	(M7 vs. M8) **12.56**** (M8 vs. M8a) **0.10**
***SCN3A* ($Na_v1.3$)**				
Nearly neutral site model (M1a)	-21487.41	18	$p_0 = 0.91$, ($p_1 = 0.09$) $\omega_0 = 0.03$, ($\omega_1 = 1.00$)	-
Site selection model (M2a)	-21487.41	20	$p_0 = 0.91$, $p_1 = 0.09$, ($p_2 = 0.00$) $\omega_0 = 0.03$, ($\omega_1 = 1.00$), $\omega_2 = 4.73$	(M2a vs. M1a) **2.92**
Site null model (M7)	-21439.44	18	$p = 0.12$, $q = 0.99$	-
Site neutral model (M8a)	-21406.75	19	$p = 0.14$, $q = 1.84$	-
Site selection model (M8)	-21401.10	20	$p_0 = 0.96$, ($p_1 = 0.04$) $p = 0.13$, $q = 1.48$ $p_0 = 0.98$, ($p_1 = 0.02$), $\omega_1 = 1.83$	(M7 vs. M8) **76.68**** (M8 vs. M8a) **11.30****
***SCN4A* ($Na_v1.4$)**				
Nearly neutral site model (M1a)	-21877.67	18	$p_0 = 0.83$, ($p_1 = 0.17$) $\omega_0 = 0.03$, ($\omega_1 = 1.00$)	-
Site selection model (M2a)	-21877.67	20	$p_0 = 0.83$, $p_1 = 0.17$, ($p_2 = 0.00$) $\omega_0 = 0.03$ ($\omega_1 = 1.00$), $\omega_2 = 123.5$	(M2a vs. M1a) **0.00**
Site null model (M7)	-21820.89	18	$p = 0.14$, $q = 0.76$	-
Site neutral model (M8a)	-21809.60	19	$p = 0.17$, $q = 1.65$	-
Site selection model (M8)	-21807.68	20	$p_0 = 0.93$, ($p_1 = 0.07$) $p = 0.16$, $q = 1.27$ $p_0 = 0.96$, ($p_1 = 0.02$), $\omega_1 = 1.51$	(M7 vs. M8) **26.42**** (M8 vs. M8a) **3.83***
***SCN5A* ($Na_v1.5$)**				
Nearly neutral site model (M1a)	-22525.65	18	$p_0 = 0.88$ ($p_1 = 0.12$) $\omega_0 = 0.04$, ($\omega_1 = 1.00$)	-
Site selection model (M2a)	-22523.34	20	$p_0 = 0.88$, $p_1 = 0.12$, ($p_2 = 0.00$) $\omega_0 = 0.03$ ($\omega_1 = 1.00$), $\omega_2 = 30.1$	(M2a vs. M1a) **4.63**
Site null model (M7)	-22482.16	18	$p = 0.15$, $q = 1.04$	-
Site neutral model (M8a)	-22465.19	19	$p = 0.20$, $q = 2.28$	-
Site selection model (M8)	-22465.19	20	$p_0 = 0.95$, ($p_1 = 0.05$) $p = 0.20$, $q = 2.28$ $p_0 = 0.95$, ($p_1 = 0.05$), $\omega_1 = 1.00$	(M7 vs. M8) **33.94**** (M8 vs. M8a) **0.00**

***SCN8A* ($Na_v1.6$)**				
Nearly neutral site model (M1a)	-18903.82	18	p_0 = 0.94 (p_1 = 0.06) ω_0 = 0.02, (ω_1 = 1.00)	-
Site selection model (M2a)	-18903.82	20	p_0 = 0.94, p_1 = 0.06, (p_2 = 0.00) ω_0 = 0.02 (ω_1 = 1.00), ω_2 = 89.1	(M2a vs. M1a) **0.00**
Site null model (M7)	-18911.33	18	p = 0.09, q = 0.99	-
Site neutral model (M8a)	-18879.57	19	p = 0.12, q = 2.25 p_0 = 0.97, (p_1 = 0.03)	-
Site selection model (M8)	-18878.56	20	p = 0.11, q = 1.70 p_0 = 0.98, (p_1 = 0.02), ω_1 = 1.42	(M7 vs. M8) **65.54**** (M8 vs. M8a) **2.02**

Table S4. Likelihood ratio tests from codeml branch and branch-site models. Included for each paralog are summaries of likelihood-ratio tests ($2\Delta\ell$) for branch and branch-site models comparing TTX-bearing newts (foreground) with other salamanders (background) using codeml from the PAML software program. Significance is indicated for p-values < 0.05 (*) and <0.01 (**) with critical values determined from the χ^2 distribution.

	ℓ	n Parameters	Parameter Estimates	$2\Delta\ell$
***SCN1A* ($Na_v1.1$)**				
One ratio model (M0)	-20546.55	17	$\omega = 0.07$	-
Branch model	-20526.69	18	ω salamanders = 0.07, ω newts = 0.17	(Branch vs. M0) **39.71****
Branch-site neutral model (A1)	-20229.55	19	$p_0 = 0.86$, $p_1 = 0.08$, ($p_2 = 0.05$) $\omega_0 = 0.03$, ($\omega_1 = 1.00$)	-
Branch-site selection model (A)	-20229.55	20	$p_0 = 0.86$, $p_1 = 0.08$, ($p_2 = 0.05$) $\omega_0 = 0.03$, ($\omega_1 = 1.00$), $\omega_2 = 1.00$	(A vs. A1) **0.00**
***SCN2A* ($Na_v1.2$)**				
One ratio model (M0)	-21838.97	17	$\omega = 0.09$	-
Branch model	-21838.97	18	ω salamanders = 0.09, ω newts = 0.09	(Branch vs. M0) **0.00**
Branch-site neutral model (A1)	-21558.98	19	$p_0 = 0.89$, $p_1 = 0.11$, ($p_2 = 0.00$) $\omega_0 = 0.05$, ($\omega_1 = 1.00$)	-
Branch-site selection model (A)	-21558.52	20	$p_0 = 0.89$, $p_1 = 0.11$, ($p_2 = 0.00$) $\omega_0 = 0.05$, ($\omega_1 = 1.00$), $\omega_2 = 7.84$	(A vs. A1) **0.94**
***SCN3A* ($Na_v1.3$)**				
One ratio model (M0)	-21867.12	17	$\omega = 0.08$	-
Branch model	-21853.31	18	ω salamanders = 0.07, ω newts = 0.15	(Branch vs. M0) **27.63****
Branch-site neutral model (A1)	-21471.92	19	$p_0 = 0.89$, $p_1 = 0.08$, ($p_2 = 0.03$) $\omega_0 = 0.03$, ($\omega_1 = 1.00$)	-
Branch-site selection model (A)	-21468.13	20	$p_0 = 0.90$, $p_1 = 0.09$, ($p_2 = 0.01$) $\omega_0 = 0.03$, ($\omega_1 = 1.00$), $\omega_2 = 5.50$	(A vs. A1) **7.59***
***SCN4A* ($Na_v1.4$)**				
One ratio model (M0)	-22400.36	17	$\omega = 0.11$	-
Branch model	-22380.87	18	ω salamanders = 0.10, ω newts = 0.25	(Branch vs. M0) **38.96****
Branch-site neutral model (A1)	-21859.15	19	$p_0 = 0.75$, $p_1 = 0.17$, ($p_2 = 0.08$) $\omega_0 = 0.03$, ($\omega_1 = 1.00$)	-
Branch-site selection model (A)	-21858.94	20	$p_0 = 0.78$, $p_1 = 0.16$, ($p_2 = 0.06$) $\omega_0 = 0.03$, ($\omega_1 = 1.00$), $\omega_2 = 1.61$	(A vs. A1) **0.42**
***SCN5A* ($Na_v1.5$)**				
One ratio model (M0)	-22980.74	17	$\omega = 0.09$	-
Branch model	-22978.73	18	ω salamanders = 0.09, ω newts = 0.12	(Branch vs. M0) **4.00**
Branch-site neutral model (A1)	-22525.65	19	$p_0 = 0.88$, $p_1 = 0.11$, ($p_2 = 0.00$) $\omega_0 = 0.02$, ($\omega_1 = 1.00$)	-
Branch-site selection model (A)	-22525.65	20	$p_0 = 0.88$, $p_1 = 0.11$, ($p_2 = 0.00$) $\omega_0 = 0.02$, ($\omega_1 = 1.00$), $\omega_2 = 66.9$	(A vs. A1) **0.00**
***SCN8A* ($Na_v1.6$)**				
One ratio model (M0)	-19187.81	17	$\omega = 0.06$	-
Branch model	-19183.65	18	ω salamanders = 0.05, ω newts = 0.09	(Branch vs. M0) **8.33***
Branch-site neutral model (A1)	-18903.82	19	$p_0 = 0.94$, $p_1 = 0.06$, ($p_2 = 0.00$) $\omega_0 = 0.02$, ($\omega_1 = 1.00$)	-
Branch-site selection model (A)	-18903.82	20	$p_0 = 0.94$, $p_1 = 0.06$, ($p_2 = 0.00$) $\omega_0 = 0.02$, ($\omega_1 = 1.00$), $\omega_2 = 1.00$	(A vs. A1) **0.00**

Table S5. Sites with elevated d_N/d_S in toxic newts. Positively selected sites were identified using branch site models from the PAML software. Numbers indicate posterior probabilities of positive selection from empirical Bayes estimates. Known TTX-binding sites are bolded. Site numbers reference amino acid positions in the rat $Na_v1.4$ channel (accession number AAA41682). Sites under putative positive selection without a homologous amino acid site in rat $Na_v1.4$ are excluded from this table.

Site	Exon	Nav1.1	Nav1.2	Nav1.3	Nav1.4	Nav1.5	Nav1.6
12	1				0.61		
27	1		0.91	0.55			
120	2					0.77	0.75
150	3				0.56		
155	3	0.53					
249	6	0.64					
278	6	0.58					
338	6			0.56			
340	6	0.79					
452	9			0.61			
460	9			0.60			
493	10	0.54					
543	13			0.98			
549	13			0.55			
621	14			0.59			
719	15			0.58			
756	**15**				**0.95**		
759	**15**			**0.61**			
767	15			0.61			
774	15			0.66			
829	16	0.53					
837	16	0.60			0.53		
842	16	0.59					
843	16			0.51			
845	16	0.60					
877	16	0.51					
879	16			0.57			
881	16	0.60					
884	16			0.97			
887	16			0.60			
898	16			0.59			
911	16	0.61					
921	16	0.51					0.74
936	16	0.53					
940	16					0.69	
946	17	0.60					
957	17	0.58					
960	17	0.59					
965	17	0.95					
968	17	0.53					
981	17				0.53		
993	18				0.53		
1006	18			0.51	0.53		
1028	18				0.98		
1046	19				0.51		
1127	20					0.56	
1179	21	0.59					
1187	21				0.52		
1189	21	0.51					
1191	21			0.86			
1194	21	0.60		0.83			
1224	21	0.61					
1240	**22**				**0.51**		
1250	22	0.61					
1254	23			0.54			
1257	23			0.97			
1261	23	0.52					
1262	23	0.61					

1367	25	0.60		
1383	25			0.52
1390	25			0.54
1519	**26**			**0.51**
1529	**26**	**0.52**		
1532	**26**			**0.98**
1542	26		0.60	
1631	26	0.52		
1719	26			0.56
1737	26		0.56	
1738	26		0.51	
1739	26	0.53		
1741	26		0.51	
1744	26		0.54	
1748	26		0.52	
1752	26		0.83	
1774	26	0.61		
1796	26	0.56		
1817	26	0.59		
1820	26	0.59		
1827	26	0.51		
1832	26	0.52		
1939	26	0.52		

Table S6. Sites under putative positive selection in all salamanders. Positively selected sites were identified using site models M2a and M8 in codeml from the PAML software. Numbers indicate posterior probabilities of positive selection from empirical Bayes estimates. A single value indicates detection from the M8 model only, and two values indicate detection from both the M2a model and M8 models. Known TTX-binding sites are bolded. Site numbers reference amino acid positions in the rat $Na_v1.4$ channel (accession number AAA41682). Sites under positive selection without a homologous amino acid site in rat $Na_v1.4$ are excluded from this table.

Site	Exon	$Na_v1.1$	$Na_v1.2$	$Na_v1.3$	$Na_v1.4$	$Na_v1.5$	$Na_v1.6$
19	1			0.58; 0.81			
22	1						0.70; 0.93
43	1			0.75; 0.95			
46	1		0.51; 0.60				
51	1				0.51		
56	1			0.56; 0.79			
73	1	0.52; 0.63		0.51		0.60; 0.84	0.68; 0.91
74	1						0.76; 0.96
80	1					0.54	
115	2				0.84		
155	3					0.52	
185	4					0.90; 0.99	
202	4			0.56			
209	5					0.62	
287	6	0.65; 0.88	0.51; 0.83				
289	6	0.54			0.74		
290	6		0.56; 0.67		0.73		
294	6	0.62; 0.85				0.52	
295	6					0.67; 0.93	
298	6	0.56; 0.78				0.51; 0.71	0.60
300	6	0.53; 0.70	0.60; 0.82				
301	6					0.56	
302	6	0.51; 0.62	0.56; 0.68	0.65; 0.88			
306	6		0.71; 0.91				
307	6			0.68; 0.92		0.53	
309	6			0.59; 0.81		0.60	
311	6					0.58	
325	6				0.80		
326	6				0.69		
328	6		0.53				
329	6			0.51; 0.66			
330	6					0.53	
332	6						0.54; 0.72
333	6	0.66		0.64; 0.88			0.56; 0.77
337	6		0.70; 0.90	0.81; 0.98			
338	6	0.55; 0.75					
339	6	0.61; 0.82	0.61; 0.75				0.57; 0.79
340	6			0.62		0.63	0.52; 0.61
344	7	0.60; 0.80	0.64; 0.82	0.51; 0.67		0.55	
345	7					0.69; 0.93	0.52; 0.61
346	7					0.69; 0.94	
348	7			0.70; 0.92		0.66; 0.90	
351	7	0.60; 0.81					
358	7	0.55; 0.71	0.58; 0.72				
365	8			0.59; 0.80		0.62; 0.88	
366	8					0.52; 0.73	
368	8	0.52; 0.70	0.56; 0.71		0.65		0.60; 0.82
374	8						0.62
401	**8**	**0.61; 0.85**		**0.51; 0.65**			**0.51; 0.68**
485	10	0.51; 0.64					
487	10	0.53; 0.71					
555	13	0.58; 0.74	0.53; 0.61	0.78; 0.97			
557	13	0.60		0.68; 0.91	0.82		0.53; 0.62
560	13	0.65					
563	13	0.66; 0.88				0.56	
567	13						0.51

598	13	0.62; 0.87			0.53	0.73; 0.96	0.57; 0.81
601	13			0.80; 0.97			
602	13					0.66; 0.91	0.65; 0.85
606	13		0.52				
609	13					0.53	
654	14			0.76; 0.96			
728	15		0.57; 0.65				
729	15			0.51; 0.64	0.89	0.50; 0.71	0.75; 0.96
732	15		0.52; 0.56	0.61; 0.81	0.64	0.71; 0.94	
739	15					0.54; 0.79	
774	15		0.70; 0.90				
828	16					0.70	
830	16						0.87; 0.99
832	16	0.55	0.57				0.85; 0.99
840	16						0.53; 0.71
841	16					0.64	
846	16					0.61	
848	16					0.57; 0.82	
849	16						0.51
850	16					0.63	
852	16			0.56; 0.69		0.55; 0.80	
864	16			0.54; 0.66			
877	16					0.68; 0.93	
878	16					0.61	
881	16					0.51	
886	16					0.52; 0.76	
887	16		0.58				
892	16				0.88		
899	16					0.54	
912	16		0.60; 0.82				
913	16		0.64; 0.82				
945	17				0.51		
947	17				0.72		
950	17					0.64	
951	17			0.73; 0.94			
952	17	0.55					
967	17	0.53; 0.70					
971	17				0.78		
972	17	0.69; 0.91			0.55		
976	17					0.53	
978	17	0.58; 0.79					
979	17			0.86; 0.99			
980	17					0.52; 0.72	
981	17	0.53; 0.71					
985	17						0.64
997	18				0.68		
999	18	0.59					
1003	18					0.61	
1004	18			0.76; 0.96			
1006	18					0.68; 0.92	
1009	18		0.64; 0.85			0.52; 0.74	0.77; 0.97
1012	18					0.52; 0.75	
1106	20					0.55; 0.79	
1111	20					0.64; 0.88	
1113	20					0.62; 0.85	
1115	20					0.65	
1187	21			0.50; 0.66			
1188	21					0.57; 0.82	
1189	21			0.54; 0.68			0.53
1192	21			0.72; 0.93			
1193	21	0.70; 0.93	0.63; 0.86	0.87; 0.99			0.73; 0.93
1195	21			0.57; 0.82	0.60		
1203	21	0.59; 0.78					0.64; 0.88
1204	21	0.58		0.53			0.69; 0.92
1207	21	0.60; 0.81		0.88; 0.99		0.61; 0.86	
1208	21			0.60; 0.81			0.55; 0.74
1211	21				0.80		
1216	21					0.58	
1251	22			0.67; 0.88			
1253	23	0.57; 0.80					

1254	23	0.59; 0.81					
1257	23				0.77		
1260	23		0.52				
1332	24	0.64; 0.85	0.53; 0.66				
1334	25		0.65; 0.87				
1351	25				0.56		
1372	25						0.69; 0.92
1380	25	0.57		0.69			
1390	25					0.62	
1533	**26**	**0.50; 0.67**	**0.55; 0.71**				
1542	26					0.66	
1543	26	0.67; 0.90				0.70	
1549	26	0.50; 0.66		0.66; 0.89	0.54		
1550	26				0.61		
1551	26		0.58; 0.78	0.68; 0.91		0.57; 0.80	
1556	26				0.84		
1558	26				0.77	0.56	
1623	26		0.56; 0.78				
1631	26			0.53			
1635	26	0.53					
1708	26				0.81		
1725	26	0.60				0.58; 0.83	
1726	26		0.62; 0.81				
1733	26	0.62; 0.81					
1736	26				0.63		
1739	26		0.56; 0.70				
1742	26				0.77		
1745	26		0.53; 0.66				
1746	26		0.70; 0.92		0.82		
1747	26		0.62; 0.83		0.74		
1748	26		0.63; 0.84				
1751	26				0.67		
1754	26				0.80		
1755	26		0.62; 0.79	0.57			
1757	26						
1767	26				0.61		
1769	26				0.61		
1775	26				0.88		
1777	26				0.50		
1784	26				0.54		
1798	26				0.88		
1800	26				0.78		
1805	26				0.58		
1807	26				0.91		
1822	26			0.58; 0.82			
1828	26					0.62	
1831	26				0.76		
1834	26				0.53; 0.93		
1835	26				0.91		

Table S8. Sources for amphibian voltage-gated sodium channel (*SCNA*) sequences used for targeted NGS sequencing probe design. WGS – whole genome shotgun database, TSA – transcriptome shotgun assembly database

Species	Source	Best BLAST hit	Accession
Ambystoma mexicanum	WGS NCBI	*SCN1A*	gb|PGSH01113157.1
Ambystoma mexicanum	WGS NCBI	*SCN2A*, *SCN3A*	gb|PGSH01109388.1
Ambystoma mexicanum	WGS NCBI	*SCN4A*	gb|PGSH01101866.1, gb|PGSH01095590.1, gb|JXRH01331098.1
Ambystoma mexicanum	WGS NCBI	*SCN5A*	gb|PGSH01008813.1
Ambystoma mexicanum	WGS NCBI	*SCN8A*	gb|PGSH01049067.1
Hynobius chinensis	TSA NCBI	*SCN1A*	gb|GAQK01012416.1, gb|GAQK01089723.1, gb|GAQK01123640.1, gb|GAQK01022956.1, gb|GAQK01037701.1, gb|GAQK01110837.1, gb|GAQK01035933.1, gb|GAQK01049457.1, gb|GAQK01026323.1 gb|GAQK01118202.1, gb|GAQK01062486.1, gb|GAQK01026323.1, gb|GAQK01062486.1
Hynobius chinensis	TSA NCBI	*SCN2A*	gb|GAQK01012415.1, gb|GAQK01089724.1, gb|GAQK01123639.1, gb|GAQK01062305.1, gb|GAQK01047585.1, gb|GAQK01096581.1, gb|GAQK01044980.1, gb|GAQK01086119.1, gb|GAQK01096592.1, gb|GAQK01106518.1, gb|GAQK01122588.1
Hynobius chinensis	TSA NCBI	*SCN4A*	gb|GAQK01140156.1, gb|GAQK01024534.1, gb|GAQK01021831.1, gb|GAQK01021830.1, gb|GAQK01082803.1, gb|GAQK01071419.1, gb|GAQK01071419.1
Hynobius chinensis	TSA NCBI	*SCN5A*	gb|GAQK01128205.1, gb|GAQK01083790.1, gb|GAQK01027263.1, gb|GAQK01027805.1, gb|GAQK01015614.1, gb|GAQK01012146.1, gb|GAQK01014539.1, gb|GAQK01014539.1
Hynobius chinensis	TSA NCBI	*SCN8A*	gb|GAQK01067521.1, gb|GAQK01020756.1, gb|GAQK01038507.1, gb|GAQK01045113.1, gb|GAQK01022217.1, gb|GAQK01096591.1, gb|GAQK01071418.1, gb|GAQK01071418.1
Hynobius retardatus	TSA NCBI	*SCN1A*	gb|LE210884.1, gb|LE107081.1, gb|LE105972.1
Hynobius retardatus	TSA NCBI	*SCN3A*	gb|LE175129.1
Hynobius retardatus	TSA NCBI	*SCN4A*	gb|LE175126.1, gb|LE175128.1

Hynobius retardatus	TSA NCBI	*SCN5A*	gb|LE143587.1, gb|LE143588.1
Hynobius retardatus	TSA NCBI	*SCN8A*	gb|LE175125.1
Lyciasalamandra atifi	Transcriptome assembly provided by Miguel Vences (Rodríguez et al. 2017)	-	-
Nanorana parkeri	WGS NCBI	*SCN1A, SCN2A, SCN3A*	gb|NW_017306417.1
Nanorana parkeri	WGS NCBI	*SCN4A*	gb|NW_017306748.1
Nanorana parkeri	WGS NCBI	*SCN5A*	gb|NW_017306389.1
Nanorana parkeri	WGS NCBI	*SCN8A*	gb|NW_017307114.1
Notophthalmus viridescens	http://sandberg.cmb.ki.se/redspottednewt/	-	-
Paramesotriton hongkonginensis	Sequence Read Archive NCBI SRX796492	-	-
Pleurodeles waltl	Whole genome assembly provided by Ahmed Elewa (Elewa et al. 2017)	*SCN1A*	abyss_v4.2_66066951
Pleurodeles waltl	Transcriptome assembly from iNewt Database: http://www.nibb.ac.jp/imori/main/	*SCN1A*	TRINITY_DN288824_c1_g3_i7
Pleurodeles waltl	Whole genome assembly provided by Ahmed Elewa (Elewa et al. 2017)	*SCN2A*	abyss_v4.2_66112789
Pleurodeles waltl	Whole genome assembly provided by Ahmed Elewa (Elewa et al. 2017)	*SCN3A*	abyss_v4.2_66060341
Pleurodeles waltl	Transcriptome assembly from iNewt Database: http://www.nibb.ac.jp/imori/main/	*SCN3A*	TRINITY_DN288824_c1_g3_i6
Pleurodeles waltl	Whole genome assembly provided by Ahmed Elewa (Elewa et al. 2017)	*SCN4A*	abyss_v4.2_48183054
Pleurodeles waltl	Transcriptome assembly from iNewt Database: http://www.nibb.ac.jp/imori/main/	*SCN4A*	TRINITY_DN288824_c1_g2_i5
Pleurodeles waltl	Whole genome assembly provided by Ahmed Elewa (Elewa et al. 2017)	*SCN5A*	abyss_v4.2_66164693
Pleurodeles waltl	Whole genome assembly provided by Ahmed Elewa (Elewa et al. 2017)	*SCN8A*	abyss_v4.2_66123907
Salamandra atra	Transcriptome assembly provided by Miguel Vences (Rodríguez et al. 2017)	-	-
Salamandra infraimmaculata	Transcriptome assembly provided by Miguel Vences (Rodríguez et al. 2017)	-	-
Salamandra salamandra	TSA NCBI	*SCN1A*	gb|GIKK01030996.1, gb|GIKK01027377.1, gb|GIKK01026170.1, gb|GIKK01027688.1
Salamandra salamandra	TSA NCBI	*SCN2A*	gb|GIKK01012950.1, gb|GIKK01007670.1, gb|GIKK01006682.1
Salamandra salamandra	TSA NCBI	*SCN3A*	gb|GIKK01031859.1
Salamandra salamandra	TSA NCBI	*SCN4A*	gb|GIKK01007017.1, gb|GIKK01015583.1
Salamandra salamandra	TSA NCBI	*SCN5A*	gb|GIKK01011042.1
Salamandra salamandra	TSA NCBI	*SCN8A*	gb|GIKK01019313.1, gb|GIKK01023854.1, gb|GIKK01002548.1

Tylototriton wenxianensis	TSA NCBI	*SCN4A*	gb|GESS01000732.1, gb|GESS01024789.1, gb|GESS01029581.1, gb|GESS01063809.1
Tylototriton wenxianensis	TSA NCBI	*SCN5A*	gb|GESS01016882.1, gb|GESS01035197.1
Xenopus tropicalis	WGS NCBI	*SCN1A*	gb|AAMC03035440.1
Xenopus tropicalis	WGS NCBI	*SCN2A*	gb|AAMC03035445.1
Xenopus tropicalis	WGS NCBI	*SCN3A*	gb|AAMC03035458.1, gb|AAMC03035459.1, gb|AAMC03035460.1
Xenopus tropicalis	WGS NCBI	*SCN4A*	gb|AAMC03036452.1
Xenopus tropicalis	WGS NCBI	*SCN5A*	gb|AAMC03022243.1, gb|AAMC03022245.1, gb|AAMC03022246.1, gb|AAMC03022247.1, gb|AAMC03022249.1, gb|AAMC03022250.1, gb|AAMC03022251.1
Xenopus tropicalis	WGS NCBI	*SCN8A*	gb|AAMC03008918.1, gb|AAMC03008917.1, gb|AAMC03008916.1